OUTP-96-10P
CERN-TH/96-162
hep-lat/9606021

Domain walls and perturbation theory in high temperature gauge theory: SU(2) in 2+1 dimensions

C. Korthals Altes[1], A. Michels[2], M. Stephanov[3], M. Teper[2]

[1] *Centre Physique Theorique au CNRS, Luminy, B.P. 907, 13288 Marseille, France*

[2] *Theoretical Physics, University of Oxford, 1 Keble Road, Oxford OX1 3NP, UK*

[3] *Department of Physics, University of Illinois at Urbana–Champaign, 1110 West Green Street, Urbana 61801, USA*

Abstract

We study the detailed properties of Z_2 domain walls in the deconfined high temperature phase of the $d = 2 + 1$ $SU(2)$ gauge theory. These walls are studied both by computer simulations of the lattice theory and by one-loop perturbative calculations. The latter are carried out both in the continuum and on the lattice. We find that leading order perturbation theory reproduces the detailed properties of these domain walls remarkably accurately even at temperatures where the effective dimensionless expansion parameter, g^2/T, is close to unity. The quantities studied include the surface tension, the action density profiles, roughening and the electric screening mass. It is only for the last quantity that we find an exception to the precocious success of perturbation theory. All this shows that, despite the presence of infrared divergences at higher orders, high-T perturbation theory can be an accurate calculational tool.

1 Introduction

Non-Abelian gauge theories possess many surprising aspects. An example is the linear confining potential present in both the three and four dimensional $SU(N)$ theories at low temperature, T. At some finite T there is a phase transition and confinement is then lost[1, 2]; but this is not unexpected because simple energy versus entropy arguments tell us that a confining 'flux tube' will condense into the vacuum at some finite value of the temperature. These phenomena are non-perturbative and have so far defied analytic, as opposed to numerical, approaches. However, at sufficiently high T, there would appear to be an important theoretical simplification. All these theories are asymptotically free so that the effective interaction on the relevant energy scale, T, should become small at high T and the physics of the gluon plasma should become accurately calculable in perturbation theory. Unfortunately there are infrared divergences in higher orders of perturbation theory, which are associated with the perturbative masslessness of the magnetic gluon. Although we expect this gluon to acquire a mass through the non-perturbative physics of the dimensionally reduced theory, this leaves room for uncertainty about how reliable high-T perturbation theory really is.

However even this naive picture of gauge theories at high T — as a weakly interacting plasma of gluons — contains surprises. There turns out to be a symmetry associated with the centre of the group, $Z(N)$, which is spontaneously broken at high T. Separating two different $Z(N)$ vacua will be a domain wall whose properties have been calculated in perturbation theory for $T \to \infty$ [3]. However the reality of these domain walls is controversial for a variety of reasons. Firstly, there are the general doubts about high-T perturbation theory that we alluded to above. Secondly, all this is in the usual Euclidean formulation of finite temperature field theories and there is a question of what if anything these domain walls might correspond to in Minkowski space-time. Finally the walls have peculiar thermodynamic properties, which become more acute when one includes quarks into the theory [4]. It is important to resolve these uncertainties not only because of the theoretical interest of these domain walls, but also because related structures can be associated with important physical phenomena when one considers the Standard Model in the early universe [5].

In this paper we address the particular problem associated with the uncertain status of perturbation theory at high T. We shall do so by calculating

the properties of the domain walls both in perturbation theory and by a fully non-perturbative Monte Carlo computer simulation. We shall work with the $SU(2)$ gauge group because the problems should not be any different for larger groups. Moreover we shall work in 2+1 dimensions rather than in the more physical case of 3+1 dimensions. The reason is that the computational resources needed are much less in the former case, and only there can we perform calculations with enough precision and control to be really useful. At the same time, the origin of the infrared problems is similar in $d = 2 + 1$ and in $d = 3 + 1$, and their severity is, if anything, greater in the lower dimensional case.

We shall find in the calculations described below that one-loop perturbation theory does indeed work remarkably — even precociously — well for our Z_2 domain walls. By implication, this provides evidence for the general applicability of perturbation theory at high T.

At the same time we emphasise that we make no attempt, in this paper, to address the other controversial aspects of domain walls and so do not attempt to settle the interesting question of their potential role in, for example, separating bubbles of different vacua in the early universe.

We shall now outline the contents of this paper. In Section 2 we give a heuristic introduction to domain walls and the thermodynamics of gauge theories at high temperatures. This will provide the general background for the more detailed and specific calculations of the later sections. We then turn to the perturbative calculation, at one-loop, of the properties of domain walls. In Section 3 we perform the calculation of the surface tension for the continuum theory. The calculation is by a method that easily extends to other dimensions and so, as well as obtaining expressions for $d = 2 + 1$, we can compare with previous $d = 3 + 1$ calculations. In order to compare with our later numerical work it is useful to have similar results for a finite value of the lattice spacing a. This calculation is carried out in Section 4. In Section 5 we calculate the action density in the domain wall, as a function of the distance from the centre of the wall, since this is one of the quantities we shall later calculate numerically. In Section 6.1 we calculate the effects of oscillations of the wall once its length is large — the 'roughening' of the wall, which has been neglected in most previous studies. In Section 6.2 we show how the finite size of the volume, in the direction orthogonal to the wall, affects the profile and surface tension of the wall. This is important to understand since our numerical work will necessarily be on lattices of a finite

size. We then turn, in Section 7, to a description of our simulations and the results we obtain thereby. We begin, in Section 7.1, by describing how we can simulate domain walls through the use of twisted boundary conditions. In Section 7.2 we point out that these domain walls can be viewed as 't Hooft disorder loops that have been squashed by the short Euclidean time direction. Section 7.3 describes how we calculate the properties of the domain wall and the electric screening mass. Section 7.4 lists the large-volume raw 'data' from which we will eventually extract physical quantities. Section 7.5 describes in detail how we control finite volume effects. This is crucial since the potential problems with perturbation theory are infrared ones. Finally, in Section 7.6 we compare our numerical results with those of perturbation theory. Section 8 contains our conclusions.

Our theoretical analysis, in Sections 3 to 6, is performed for the general case of $SU(N)$ gauge fields in $2 < d \leq 4$ dimensions. Our numerical results, on the other hand, are for the particular case of $SU(2)$ gauge fields in $d = 2 + 1$. The preliminary results of this study appeared in the Proceedings of the 1994 Lattice Conference [6]. A study of the case of $SU(3)$ gauge fields in $d = 2 + 1$ has recently been reported [7]. Both the $SU(2)$ and $SU(3)$ results are in agreement with our theoretical analysis. In addition both show the same large deviation from D'Hoker's self-consistent formula for the Debye mass.

2 General considerations

In 2+1 dimensions the gauge coupling, g^2, is dimensionful and its value sets the mass scale for the theory. If we perform a perturbative calculation of a quantity in which there is a dominant momentum scale, Q, then the effective expansion parameter will clearly be g^2/Q so that the theory rapidly becomes free at short distances. So at high T the effective expansion parameter, g^2/T, will be small and we can expect that we should be able to apply perturbation theory. All this is very similar to the case in 3+1 dimensions. There the coupling is dimensionless but this difference is only apparent: the scale-invariance is anomalous, the coupling runs and its value only serves to set the overall mass scale (dimensional transmutation). The coupling becomes small at short distances, so that its value at high temperature, $g^2(T)$, should be small enough for us to apply perturbation theory. In other

ways the two theories are also similar: numerical simulations [25] show that the $d = 2 + 1$ theory has linear confinement, a deconfining temperature, T_c, and a glueball spectrum that are similar in many ways to that of the theory in 3+1 dimensions.

So we expect a hot gauge theory to be, to a very good approximation, a plasma of free gluons, with interactions given in terms of the small effective coupling at the ambient temperature T. These gluons are screened just as are photons in a plasma of charged particles. The Debye screening mass, m_D, that they acquire grows with T; to lowest order ${m^2}_D$ is $O(g^2)$ so we expect, on purely dimensional grounds, that $m_D \sim g(T)T$ in $d = 3 + 1$ and $m_D \sim gT^{1/2}$ in $d = 2 + 1$.

However this simple picture is not the whole story. An additional and important role is played by the center, $Z(N)$, of the gauge symmetry group $SU(N)$. This sub-group has a special status because the gluons, which transform according to the adjoint representation, are invariant under gauge transformations that belong to the centre. Since the gluons only feel $SU(N)$ gauge transformations modulo any $Z(N)$ transformation, their symmetry group is really $SU(N)/Z(N)$. Sources in the fundamental representation, on the other hand, are not invariant under transformations in $Z(N)$. Consider such a heavy source in the usual Euclidean space-time formulation of the high-T field theory where the Euclidean time is periodic with period $1/T$. As is well known the presence of such a static heavy source leads to an extra factor of $P \equiv (1/N)\ \mathrm{tr}\ \mathrm{P} \exp\{i \int A_0 dt\}$ — a Polyakov loop — in the partition function. In the low T confining phase $\langle P \rangle = 0$ while at high T $|\langle P \rangle| \simeq 1$. Since the gluons are screened, the correlations are short range at high T and so if, for example, P is close to 1 at one point, the vacuum will have $P \simeq 1$ everywhere. But the $Z(N)$ symmetry tells us that there must be N such vacua, in each of which the physics is identical, and which are differentiated by P being close to one of the N complex N'th roots of unity. The picking of one of these vacua corresponds to the spontaneous breaking of the symmetry. That the spontaneous breaking takes place at high T rather than at low T is remarkable but not impossible; it is, for example, a commonplace in (self-)dual theories.

As soon as we have spontaneous symmetry breaking we have the possibility of domain walls which will occur at the interface between two of the vacua. (Throughout this paper we shall call these objects 'walls', and will speak of their 'surface' tension, even though the interface is really a string

when we are in 2 spatial dimensions. This is to avoid confusion with the confining string.) In the case of interest to us, $SU(2)$, such a domain wall would separate regions of our Euclidean space-time volume that are characterised by $P \simeq +1$ on the one side and $P \simeq -1$ on the other. One can compute the free energy density of the wall for small coupling and one indeed finds a positive excess over the free energy of the gluon plasma.

Thus we have a picture of the gluon plasma that parallels that of a ferro-magnetic substance below the Curie temperature: the average of the Polyakov loop, which arises from the heavy fundamental source, being the order parameter. But what is the analogue of the external field? Such a field is needed in order to make the system choose a particular direction of magnetisation on a macroscopic scale. Without such an analogue one cannot trigger a thermodynamical state where our order parameter, P, takes the value $+1$ or one where it takes the value -1.

As we remarked in the Introduction, the 'reality' of these domain walls is controversial. Of course, the walls have been observed [8] in $(d = 3 + 1)$ Monte Carlo simulations of the theory, but this has only been for large lattice spacings, and there have been speculations that the walls would not survive into the continuum limit [9]. In this paper we shall address the question of whether these domain walls do indeed exist in the continuum limit and, more specifically, whether high-T perturbation theory is reliable. But first, in this section, we introduce the basic framework within which we work.

2.1 Yang-Mills fields: the basic parameters

We consider a pure $SU(N)$ gauge theory in 2 or 3 space dimensions. We will concentrate in this subsection on the thermodynamic quantities that one can define by enclosing the system in a box of size $L_y L_z$. (For the three-dimensional case we add an x-direction.) The Hamiltonian for this system reads:

$$\hat{H} \equiv \frac{1}{2} \int_{\boldsymbol{x}} \ \mathrm{tr}\Big(g^2 \hat{\boldsymbol{E}}^2 + \frac{1}{g^2} \hat{\boldsymbol{B}}^2 \Big), \tag{1}$$

where $\hat{\boldsymbol{E}}$ is the canonical momentum for $\hat{\boldsymbol{A}}$ and $\hat{B}_{mn} \equiv \partial_m \hat{A}_n - \partial_n \hat{A}_m + i[\hat{A}_m, \hat{A}_n]$. We use the standard notation for the fields as $N \times N$ matrices in the Lie algebra of the defining representation of $SU(N)$.

We introduce the free energy F of the system in a heat bath at temperature T through the Gibbs trace over the physical states of the system. By

'physical' we mean that the states obey the Gauss constraint

$$\left(\boldsymbol{\nabla}\hat{\boldsymbol{E}} + i[\hat{\boldsymbol{A}}, \hat{\boldsymbol{E}}]\right)|\psi\rangle = 0. \tag{2}$$

The free energy is defined by

$$\exp\left(-\frac{F}{T}\right) = \mathrm{Tr}_{\mathrm{phys}} \exp\left(-\frac{\hat{H}}{T}\right). \tag{3}$$

As is well known, the Gibbs trace can be related to the Feynman path integral by

$$\mathrm{Tr}_{\mathrm{phys}} \exp\left(-\frac{\hat{H}}{T}\right) = \int \mathcal{D}A_0 \mathcal{D}\boldsymbol{A} \exp\left\{-\frac{1}{g^2}S(A)\right\}. \tag{4}$$

Here the integration over A_0 implements the Gauss law, the action $S(A)$ is equal to $(1/4)\int d\boldsymbol{x}dt\ \mathrm{tr}F_{\mu\nu}F_{\mu\nu}$, and the temperature enters the formalism through the fact that we make the potentials periodic in the Euclidean time t with period $1/T$. The relationship (4) is fundamental in that it allows us to calculate the free energy using the whole panoply of methods available for calculating path integrals; such as perturbation theory(see Sections 3 and 4) and Monte Carlo methods (see Section 7).

Throughout this paper we suppose the potentials to be periodic in the spatial directions. However, this does not mean that any gauge transformation Λ has to be periodic, only that it should be periodic modulo an element, $z_k = \exp\{ik\frac{2\pi}{N}\}$, of the centre $Z(N)$ of $SU(N)$. That this is so is easily seen from the transformation properties of the potential:

$$A_\mu^\Lambda = \Lambda^\dagger A_\mu \Lambda - i\Lambda^\dagger \partial_\mu \Lambda. \tag{5}$$

If say $\Lambda(L_z) = \Lambda(0)z_k$, then the z_k will commute with all the matrices in (5) and so will disappear from the right hand side, leaving the transformed potential still periodic [10]. We shall denote such gauge transformations by $\hat{\Lambda}_{\boldsymbol{k}}$. If $\boldsymbol{k} = (k_y, k_z)$ then this is a gauge transformation which is periodic up to z_{k_y} in the y-direction and up to z_{k_z} in the z-direction.

The interest of these extended gauge transformations lies in two facts:

- they leave the Hamiltonian (1) invariant;
- they serve to distinguish subspaces, in the space of physical states, which possess a given number, e_y and e_z, of electric fluxes in the y and z directions respectively. Clearly this distinction is modulo N.

The above notion of electric flux is developed in detail in [10]. The following remarks represent no more than a heuristic outline. Suppose first that we have opposite fundamental sources at $\boldsymbol{x}_1$ and $\boldsymbol{x}_2$. To make this system gauge invariant we need to join the sources by a finite string $\mathrm{P}\exp\{i\int_{\boldsymbol{x}_1}^{\boldsymbol{x}_2}\hat{\boldsymbol{A}}d\boldsymbol{x}\}$ running between them. Such a string operator creates the unit fundamental (electric) flux that must flow between the sources. Suppose we are now in the purely gluonic system with no sources and suppose we wish to add a unit of electric flux across the whole volume, running in the z-direction. From the above we expect that we can do so by applying to our state the periodic string operator $\mathrm{tr}\,\mathrm{P}\exp\{i\int_0^{L_z}dz\hat{A}_z\}$. Unlike a contractible string operator loop, which would represent some local excitation, this operator will clearly feel the centre element of the gauge transformation $\hat{\Lambda}_{\boldsymbol{k}}$ if $k_z\neq 0$. Indeed it is easy to see that it will acquire a factor of z_{k_z}. If we create a state with n such units of electric flux in the z-direction, then it will acquire a factor of $(z_{k_z})^n$. So if we label a state with electric flux $\boldsymbol{e}=(e_y,e_z)$ by $|\boldsymbol{e}\rangle$, it will be an eigenstate of $\hat{\Lambda}_{\boldsymbol{k}}$ with eigenvalue $\exp\{i\boldsymbol{k}\cdot\boldsymbol{e}\frac{2\pi}{N}\}$, (assuming trivial transformation properties for the fluxless state $|\boldsymbol{0}\rangle$). Clearly the state with $N+1$ fluxes has the same transformation property as that with 1 unit of flux; as one would expect in a non-Abelian theory.

Since the Hamiltonian is invariant under $\hat{\Lambda}_{\boldsymbol{k}}$, the energy eigenstates can be simultaneously labeled by $\boldsymbol{e}$ and we can define a free energy $F\boldsymbol{e}$ by restricting the Gibbs trace in (3) to a given electric flux sector:

$$\exp\left(-\frac{F\boldsymbol{e}}{T}\right)=\mathrm{Tr}_{\boldsymbol{e}}\exp\left(-\frac{\hat{H}}{T}\right) \tag{6}$$

With this definition relation (3) can be rewritten as [10]:

$$\exp\left(-\frac{F\boldsymbol{e}}{T}\right)=\frac{1}{N^{d-1}}\sum_{\boldsymbol{k}}\exp\left\{-i\boldsymbol{k}\cdot\boldsymbol{e}\frac{2\pi}{N}\right\}Z_{\boldsymbol{k}}, \tag{7}$$

where

$$Z_{\boldsymbol{k}}\equiv\mathrm{Tr}_{\mathrm{phys}}\exp\left(-\frac{\hat{H}}{T}\hat{\Lambda}_{\boldsymbol{k}}\right). \tag{8}$$

The Gibbs traces $Z_{\boldsymbol{k}}$ in (8) can be expressed as "twisted" path integrals and can be computed using Monte Carlo methods. These path integrals have the following defining property. Suppose, for example, that $\boldsymbol{k}=(0,k_z)$. Then

due to the occurrence of the transformation $\hat{\Lambda}_{\boldsymbol{k}}$ in (8) one picks up a factor of $\exp\{ik_z 2\pi/N\}$ in the gauge transform relating $A(t,y,0)$ to $A(t,y,L_z)$ and $A(0,y,z)$ to $A(L_t,y,z)$, after going around the boundary of the box in the z-t directions. This multivaluedness does not affect the gluon field A_μ. In Section 7 we will perform Monte Carlo simulations of such a twisted partition function.

2.2 The two important parameters: string and surface tension

Now we are ready to give a thermodynamic characterisation of the various phases of the gauge theory, through the behaviour of the flux free energies $F_{\boldsymbol{e}}$ as the temperature is varied. To obtain simple formulas we will restrict ourselves to $SU(2)$, but the end results will be valid for any $SU(N)$. The interesting quantity is the flux free energy F_{01} in the elongated direction. We want to compare it to the flux free energy F_{00} and see how the difference behaves for low and high temperatures. This is straightforward using (7) for the flux free energies. But we still need some theoretical input on how the twisted functionals behave. What one finds for low T is that

$$1 - \frac{Z_{01}}{Z_{00}} = C \exp\left(-\frac{\rho(T)}{T} L_z\right), \tag{9}$$

while $1 - (Z_{k_y 1}/Z_{00})$ is exponentially smaller for any $k_y \neq 0$. On the other hand for high enough T one finds:

$$Z_{01} = D \exp\left(-\frac{\sigma(T)}{T} L_y\right) Z_{00} \tag{10}$$

and $Z_{k_y 1}$ is exponentially smaller for any $k_y \neq 0$. The C and D are some pre-exponential factors. The evidence for (9) and (10) comes from Monte Carlo simulations, as well as analytic Hamiltonian analyses of gauge Potts models [11]. So one gets for the free energy difference:

$$F_{01} - F_{00} \sim \rho(T) L_z \qquad \text{if } T \text{ is small} \tag{11}$$

$$F_{01} - F_{00} \sim L_z \exp\left\{-\frac{\sigma(T)}{T} L_y\right\} \qquad \text{if } T \text{ is large} \tag{12}$$

Clearly what (11) is telling us is that at low temperatures we are in a confining regime, where imposing unit electric flux across the lattice costs us an energy that is proportional to the length traversed by the flux; and the tension of this flux 'string' is ρ. So the free energy difference becomes very large at large L_z, but is insensitive to the transverse spatial dimensions. At some critical temperature T_c this behaviour changes into that of (12). The free energy difference now becomes exponentially small with the transverse size. This behaviour suggests that there is a wall, with an energy density independent of the transverse direction, and a total energy proportional to σ. This quantity has been computed in a semiclassical approximation [3, 12] at very high temperatures, where perturbation theory should apply. The purpose of the present study is to check the validity of this approximation using Monte Carlo methods.

The way the surface tension enters the free energy difference is through the exponential. This was first noticed by Bhattacharya et al. [13] and was recently discussed in a $Z(2)$ gauge model [14]. It is reminiscent of an energy difference induced by tunneling. As we will see in the next section this is indeed a tunneling through a potential that arise from quantum one-loop effects.

2.3 Effective Action and Polyakov Loops

As we have seen above, the fundamental quantity of interest is the ratio of twisted path integrals $Z_{\boldsymbol{k}}$. These are computed by converting from the vector potentials, as integration variables, to Polyakov loops:

$$\Omega(\boldsymbol{x}) \equiv \ \mathrm{P} \exp\left\{ i \int_0^{1/T} dt A_0(t, \boldsymbol{x}) \right\} \tag{13}$$

and by integrating out the remaining variables to get an effective action for $\Omega(\boldsymbol{x})$. In a suggestive notation:

$$\exp\{-S_{\mathrm{eff}}(\Omega)\} = \int \mathcal{D}A \, \delta \left[\Omega - \ \mathrm{P} \exp\left\{ i \int_0^{1/T} dt A_0 \right\} \right] \ \exp\left\{ -\frac{1}{g^2} S(A) \right\} \tag{14}$$

The reader, in looking at this equation, should keep in mind that only the eigenvalues λ_i of the loop Ω are gauge invariant. So it is only these that

should appear in the delta function constraint and in $S_{\rm eff}$. Note also the relation between Ω and P:

$$P = \frac{1}{N}\ {\rm tr}\Omega = \frac{1}{N}\sum_i \lambda_i. \tag{15}$$

The $S_{\rm eff}$ has been worked out [13, 12, 15] to two loop order in the $d = 3 + 1$ case. In Section 3 we will derive the one loop result for any d, and in particular for the case of interest in this paper, $d = 2 + 1$.

It is important to note that the effective action does not depend on the boundary conditions if the volume is large enough. It is also easy to see that the twist $\boldsymbol{k} = (0, k_z)$ of the previous section corresponds to the following boundary conditions in the effective theory for $\Omega(y, z)$:

$$\Omega(y, L_z) = \exp\{ik_z\frac{2\pi}{N}\}\Omega(y, 0). \tag{16}$$

With such boundary conditions $Z_{\boldsymbol{k}}$ is given by:

$$Z_{\boldsymbol{k}} = \int_{(\boldsymbol{k})} \mathcal{D}\Omega\ \exp\left(-S_{\rm eff}(\Omega)\right). \tag{17}$$

We also note that the path integral has a formal resemblance to that of a spin model partition function. The effective action, when evaluated in perturbation theory, will start with a classical kinetic term. The first non-zero contribution for constant $\Omega(\boldsymbol{x})$ appears at one-loop. So to this order we can write:

$$S_{\rm eff}(\Omega) = \int_{\boldsymbol{x}} {\rm tr}\left[\frac{T}{2g^2}|\boldsymbol{\nabla}\Omega|^2 + V_{\rm eff}(\Omega)\right], \tag{18}$$

At high T the coefficient of the gradient term is large and we can expect that the path integral will be saturated by smooth configurations of Polyakov loops. We shall see in the next section that $V_{\rm eff}$ reaches its minima when all N eigenvalues of Ω coincide. Due to a condition $\det\Omega = 1$ there are N such minima: $\Omega \in Z(N)$. The order parameter distinguishing between these N degenerate phases is the value of the Polyakov loop P (15). The $Z(N)$ symmetry in the effective theory of Polyakov loops is due to the existence of gauge transformations which are periodic in the Euclidean t direction up to an element of $Z(N)$: $\Lambda(1/T) = \Lambda(0)z_k$. These transformations leave $S(A)$ invariant but multiply Polyakov loops by z_k.

In spin model language, we are in an ordered phase when T is large. This is a phase in which the entropy of the spin system is low. However the spin system is, at the same time, supposed to be describing a very hot gauge system with a large entropy in terms of quantum states. It is this complementary feature of the spin and gauge systems, that has given rise to a lot of confusion in the past few years. For example, one can ask the following question: what is the meaning of a localised surface in the spin model in terms of the gauge model? In this paper we will not go into this question, but take the pragmatic point of view that we just want to calculate the exponent in the decay law (12) for the hot fluxes. Nonetheless, one should bear in mind, that if one does assume the existence of a well localised interface, this leads to unusual thermodynamic properties; as we shall see below.

2.4 Some Thermodynamic Properties of the Wall in Gauge Theory

The study of surface effects requires a careful specification of boundary conditions. Only when that is done can we separate the free energy of the system into well defined bulk and surface free energies. Let us suppose we have in our two dimensional 'box' a domain wall, separating two domains. Then the free energy F will be for large L_y and L_z:

$$F = fL_yL_z + \sigma L_y \tag{19}$$

Here we assume that the size of the box is much larger than any of the microscopic quantities in the system.

What this equation describes is simply a wall with a constant free energy density in the y- direction, and a non-trivial free energy profile in the z-direction. When integrated over z, this profile gives the interface tension σ. This profile is like a soliton.

In our three dimensional $SU(2)$ gauge theory we have a dimensionful coupling constant g, with dimension $\sqrt{\text{mass}}$. The only other dimensionful quantity in our problem is the temperature T. We will typically work in the regime where g^2/T is a small number. So on the basis of dimensions alone the interface tension has a simple form:

$$\sigma = a(g^2/T)T^2 \tag{20}$$

with function a positive and dimensionless. We can apply semi-classical methods to calculate a. These methods typically give, when applied to solitons such as monopoles and sphalerons,

$$E_{\rm sol} \sim \frac{\rm scale}{\rm coupling} \tag{21}$$

for the energy $E_{\rm sol}$ in terms of the scale (Higgs expectation value). So it is not surprising that we obtain, as described in detail in the next section, a similar result for our profile:

$$\sigma = \alpha_0 \frac{T^2}{\frac{g}{\sqrt{T}}} = \alpha_0 \frac{T^{5/2}}{g}. \tag{22}$$

where α is a numerical factor of geometrical origin. The expression (22) can be easily understood if one realizes that the domain wall has a width w of the order of the screening length $w \sim 1/(gT^{1/2})$, carries an excess of free energy density $\Delta f \sim T^3$ and that $\sigma \sim w\Delta f$.

We are now ready for the following thermodynamical observations. First consider a droplet of radius R of 'minus' phase in a sea of 'plus' phase. The free energy excess due to the presence of this droplet equals

$$\Delta F = 2\pi R\sigma. \tag{23}$$

Now, the probability for the appearance of such a droplet is $\exp\{-\Delta F/T\}$. From the explicit dependence of σ on T we learn that this probability becomes exponentially small for *large* T. So we find that an ordered phase prevails at high temperature[1].

The second observation is a simple consequence of the positivity and the explicit temperature dependence of the interface tension. The interface entropy equals

$$\text{entropy} = -\frac{\partial}{\partial T}\sigma = -\frac{5}{2}\alpha_0 \frac{T^{3/2}}{g} \tag{24}$$

So the interface entropy is negative! As is the interface internal energy ϵ, although the free energy given by the difference $-T\sigma$ is positive. Such a

[1] A study of discrete gauge models reveals the same phenomenon: they can be mapped onto a two dimensional Ising model with a coupling $\sim \log T$ for T large. That is, for T large both models start to order.

negative interface entropy is to be expected quite generally for models that order at high temperature: the free energy starts to *grow* at the critical temperature, and consequently the entropy is negative. So the presence of the wall diminishes the entropy of the system.

3 Continuum calculation

In this section we calculate $S_{\rm eff}$, the surface tension and the profile of the order parameter (Polyakov loop) of the $Z(N)$ wall. When the temperature is high the effective gauge coupling becomes small and one can use perturbation theory to calculate the effective action (18). This has been done by several authors [16, 17] for $d = 4$. Here we derive similar results for $d = 3$. Our method is simpler and is trivially generalized to arbitrary d. The lattice version of these results is presented in Section 4.

We start from the partition function of the pure gauge theory at finite temperature:

$$\begin{aligned} Z &= \int \mathcal{D}A_\mu \exp\left\{-\frac{1}{4g^2}\int_0^{1/T} dt \int_{\boldsymbol{x}} \mathrm{tr}\, F_{\mu\nu}F_{\mu\nu}\right\} \\ &= \int \mathcal{D}A_0 \mathcal{D}\boldsymbol{A} \exp\left\{-\frac{1}{2g^2}\int_0^{1/T} dt \int_{\boldsymbol{x}} \mathrm{tr}\left[(\partial_0 \boldsymbol{A} + \boldsymbol{D}A_0)^2 + \boldsymbol{B}^2\right]\right\} \end{aligned} \quad (25)$$

We use some obvious short hand notations. The gauge potentials: $A_\mu \equiv iA_\mu^a T^a$ and the hermitian generators of the $SU(N)$ group are normalized as: $\mathrm{tr}\, T^a T^b = \delta^{ab}$. The covariant derivative is:

$$\boldsymbol{D}A_0 \equiv \boldsymbol{\nabla}A_0 + i[\boldsymbol{A}, A_0]. \quad (26)$$

Bold symbols denote vectors ($d-1$ components). The exception is $\boldsymbol{B}$ which is an antisymmetric tensor ($(d-1)(d-2)/2$ components):

$$B_{ik} = \partial_i A_k - \partial_k A_i + i[A_i, A_k] \quad (27)$$

In contrast to [16, 17] we do not begin by fixing the gauge. First we rewrite the partition function in the form of an integral over physical fluctuations at very high T. These are the transverse components of the vector potential $\boldsymbol{A}$. To achieve this we integrate over A_0 which is clearly an auxiliary field.

For every given configuration $\boldsymbol{A}(\boldsymbol{x},t)$ we can do this easily: the integral is Gaussian. We obtain:

$$Z = \int \mathcal{D}\boldsymbol{A}\, \det(-\boldsymbol{D}^2)^{-1/2} \\ \times \exp\left\{-\frac{1}{2g^2}\int_0^{1/T} dt \int_{\boldsymbol{x}} \mathrm{tr}\left[(\partial_0 \boldsymbol{A} - \boldsymbol{D}\boldsymbol{D}^{-2}\boldsymbol{D}\partial_0\boldsymbol{A})^2 + \boldsymbol{B}^2\right]\right\} \quad (28)$$

Thus far our manipulations have been exact. Now we use the smallness of g. In the leading order in g (saddle point approximation) we need to keep only terms quadratic in $\boldsymbol{A}$ in the exponent and can neglect the pre-exponent. As expected the effect of A_0 is to project out the longitudinal fluctuations of $\boldsymbol{A}$ from the kinetic term in (28). The $\boldsymbol{B}^2$ term does not contain them already. We see that the integral over $\boldsymbol{A}$ factorises into integrals over $d-2$ (times N^2-1) transversal fluctuations and a trivial infinite factor.

Each of these integrals represents a very well known partition function of the photon gas, the logarithm of which is:

$$\ln Z_0 = (d-2)\ln\det(-\partial_0^2 - \boldsymbol{\nabla}^2)^{-1/2} \\ = -(d-2)\int \frac{\mathcal{V} d^{d-1}\boldsymbol{k}}{(2\pi)^{d-1}} \ln(1-\exp\{-|\boldsymbol{k}|/T\}), \quad (29)$$

where $\mathcal{V}$ is the volume of space. Thus we obtain the Stefan-Boltzmann law for the free energy density of the hot gluon gas (with a multiplicity of 'photons' N^2-1):

$$\mathcal{F} = -(N^2-1)\frac{T}{\mathcal{V}}\ln Z_0 = -cT^d, \quad (30)$$

where c is:

$$c = (N^2-1)(d-2)\frac{\Gamma(d/2)}{\pi^{d/2}}\zeta(d). \quad (31)$$

Next, we want to find the dependence of the free energy density on the value of the Polyakov loop. To this end we calculate the partition function (25) about a constant background field $\underline{A}_0$. We make a shift: $A_0 = A_0' + \underline{A}_0$ and integrate over A_0'. This results in simply replacing $\partial_0\boldsymbol{A}$ with

$$\partial_0\boldsymbol{A} + i[\underline{A}_0, \boldsymbol{A}] \quad (32)$$

in equation (28). For a given matrix $\underline{A}_0$ there will be at least $N-1$ generators that commute with it ('neutral') and at most $N(N-1)$ that do not

('charged'). The 'charges' are given by: $q_i - q_j$, where q_i are the eigenvalues of the matrix $\underline{A}_0/(2\pi T)$. These are related to the eigenvalues λ_i of the Polyakov loop Ω (13) by: $\lambda_i = \exp\{i2\pi q_i\}$. The contribution of 'neutral' bosons is unchanged by (32) and is still given by (29). The partition function of the 'charged' gluons is given by:

$$\begin{aligned}\ln Z_q &= (d-2)\ln\det(-(\partial_0 + i2\pi qT)^2 - \boldsymbol{\nabla}^2)^{-1/2} \\ &= -(d-2)\int \frac{\mathcal{V}d^{d-1}\boldsymbol{k}}{(2\pi)^{d-1}}\ln(1-\exp\{-|\boldsymbol{k}|/T + i2\pi q\}). \end{aligned} \tag{33}$$

where $q = q_i - q_j$. The periodicity in q reflects the $Z(N)$ symmetry.

Following [13] we choose $q_1 = ... = q_{N-1} = q/N$. Only $N-1$ eigenvalues are independent: $\sum_i q_i = 0$ and thus $q_N = q/N - q$. As q varies from 0 to 1 the Polyakov loop:

$$P = \frac{1}{N}\ \mathrm{tr}\exp\left\{\frac{i}{T}\,\underline{A}_0\right\} \tag{34}$$

changes from 1 to $\exp(i2\pi/N)$. In the $SU(2)$ case q parameterises the only path between the two minima of the effective potential for the Polyakov loop. In $SU(3)$ it parametrises the lowest action path [12]. It is possible that it does the same for $N > 3$.

With our choice of $\underline{A}_0$ there are $(N-1)^2$ 'neutral' gluons and $2(N-1)$ gluons with 'charges' equal to $\pm q$. The free energy density as a function of the Polyakov loop order parameter (parameterised by q) is now given by:

$$\mathcal{F}(q) = -cT^d + V(q)T^d \tag{35}$$

All the dependence on q comes from the 'charged' gluons and is given by the universal function:

$$\begin{aligned}V(q) &= -2(N-1)(d-2)\int \frac{d^{d-1}\boldsymbol{k}}{(2\pi T)^{d-1}}\ln(1-\exp\{-|\boldsymbol{k}|/T\}(1-\cos 2\pi q)) \\ &= 2(N-1)(d-2)\frac{\Gamma(d/2)}{\pi^{d/2}}\sum_{\nu=1}^{\infty}\frac{1}{\nu^d}(1-\cos 2\pi q\nu). \end{aligned} \tag{36}$$

For $d = 4$ this function is expressed via the Bernoulli polynomial $B_4(q)$. For $d = 3$ only a numerical evaluation is possible.

For q varying slowly on the scale of $1/T$ one can use the tree expression for the gradient term [12]. Then the free energy density reads:

$$\mathcal{F}(q) = \frac{N-1}{N}\left(\frac{2\pi T}{g}\boldsymbol{\nabla} q\right)^2 + (V(q)-c)T^d \equiv T^d\left[\frac{\gamma^2}{2}(\boldsymbol{\nabla} q)^2 + V(q) - c\right] \tag{37}$$

where we defined a dimensionful parameter γ:

$$\gamma = \sqrt{\frac{N-1}{N}}\sqrt{\frac{8\pi^2}{g^2 T^{d-2}}}. \tag{38}$$

This completes the calculation of $S_{\rm eff}$ of Section 2.3: $S_{\rm eff} = \int_{\boldsymbol{x}} \mathcal{F}/T$.

The profile of the wall between phases with $q(-\infty) = 0$ and $q(\infty) = 1$ is given by the function $q_0(z)$ which minimizes (37) under corresponding boundary conditions. It satisfies:

$$\gamma\frac{dq(z)}{dz} = \sqrt{2V(q)}. \tag{39}$$

The width of the wall is controlled by γ: $w \sim \gamma \sim 1/(gT^{d/2-1})$. The exact solution $q_0(z)$ for $d = 4$ is known [12]. For $d = 3$ we solve (39) numerically. The surface tension σ is given by the integral of the excess of the free energy density inside the wall and is proportional to the action on the trajectory $q_0(z)$:

$$\sigma = T^d\int dz\, 2V(q_0(z)) = \gamma T^d\int_0^1 dq\,\sqrt{2V(q)} = \alpha_0\frac{T^{d/2+1}}{g}, \tag{40}$$

where we defined:

$$\alpha_0 \equiv 4\pi\sqrt{\frac{N-1}{N}}\int_0^1 dq\sqrt{V(q)}. \tag{41}$$

For $d = 3$ and $N = 2$ we find using (36): $\alpha_0 = 5.104$.

An interesting property of $d = 3$ is that the second derivative of $V(q)$ diverges at $q = 0 \bmod 1$ (see (36)). In fact, $V(q) \propto q^2\ln(1/q)$ rather than q^2 for small q. One can see from (39) that this results in a Gaussian rather than exponential fall-off in the tails of the solution. This is related to the fact that the Debye mass in the Thomas-Fermi approximation is divergent in $d = 3$ if the charged particles are massless: the well-known $\int d\boldsymbol{k}^2/\boldsymbol{k}^2$. On

the other hand, D'Hoker argued [18] that *all* infrared divergences in QCD_3^T are cut off by a Debye mass m_D of order $g\sqrt{T\ln(T/g^2)}$ (see eq. (117)). This means that the fast Gaussian fall-off should saturate at the exponential when q gets small enough ($2\pi qT \ll m_D$) , i.e., sufficiently far from the center of the wall.[2] This behavior of the tail does indeed occur in our Monte Carlo study (see Section 7.5).

4 Lattice version of the interface tension calculation

To compare numerical lattice data with theory requires a lattice version of the calculation of the previous section.

In this section we develop a one loop expression on a lattice with L_t sites in the temperature direction and an infinite number in all space directions. Quantities computed in this section are the effective potential, the profile of the wall, and the surface tension. In Section 5 we calculate the expectation values of electric and magnetic plaquettes. In Section 6 the reader will find estimates of finite size corrections. In the dimensionality we are interested in we have to go to higher loops to get a finite Debye mass. We follow to this end the ideas of D'Hoker [18], which amount to a very simple prescription.

Let us first fix our notation. The continuum action of Section 3 becomes on the lattice [19]:

$$\frac{1}{g^2}S_{\rm cont} \to \beta S_{\rm lat} = \beta \sum_p {\rm Re}[1 - \frac{1}{N}{\rm tr}U_p] \tag{42}$$

Here every plaquette p is summed over only once; in contrast to the continuum action where the sum over μ, ν included both orders.

The lattice spacing a is related to the temperature T by

$$aL_t = \frac{1}{T} \tag{43}$$

which follows immediately from the fact that the length of the system in the fourth direction is $1/T$.

[2] This happens, however, beyond the applicability of our formulas for $q(z)$.

The lattice action should become the continuum action in the limit where the dimensionless quantity aA_μ becomes very small:

$$U_P \sim \exp\{ia^2 F_{\mu,\nu}\}. \tag{44}$$

The lattice coupling becomes in that limit:

$$\frac{\beta}{2N} = \frac{a^{d-4}}{g^2} \tag{45}$$

or

$$\frac{\beta}{2N} L_t^{4-d} = \frac{T^{4-d}}{g^2} \tag{46}$$

This is the relation between lattice and continuum parameters in any number of dimensions d. For $d = 4$ all reference to dimensionful properties drops out. Perturbation theory is defined by taking the dimensionless parameter $g^2 T^{4-d}$ small, or β large at fixed L_t.

First we need a definition of the surface tension on the lattice. This can be done by taking the lattice analogues of twisted and untwisted boxes and their corresponding partition functions. This corresponds precisely to the way we measure the surface tension on the lattice (see section 7):

$$\exp\left\{-\frac{\sigma}{T} L^{d-2}\right\} \equiv \frac{Z(\text{twisted})}{Z(\text{untwisted})}. \tag{47}$$

Although our aim is to study a continuum theory, all our Monte Carlo results come from a lattice with finite lattice spacing a. The value of a has a meaning only in comparison with physical length parameters. For our system there are two such parameters: the inverse temperature $1/T$ and the Debye length, or the width of the wall w. The width $w \sim 1/(gT^{d/2-1})$ is large compared to $1/T$ for small g. To the order we are interested in we can neglect corrections due to finiteness of the ratio of w over $1/T$ or a. We choose large β so that the ratio w/a is big: $10 - 20$, and we neglect corrections due to its finiteness.[3]

However, to save computer time we choose to keep the ratio of $1/T$ to a relatively small. This ratio is the number of lattice sites in the temporal direction: L_t. To compare with our MC data we calculate the quantities discussed in Section 3 for *any* L_t to the leading order in g.

[3]We study the corrections due to the finiteness of L_z/w in Section 6.2.

To achieve this we notice, that to the order we are working in we have a theory of free gluons interacting only with the background. All path integrals are Gaussian and factorise into integrals over momentum modes. We need only to substitute the lattice periodic momenta for continuum ones:

$$k_i \longrightarrow \frac{2}{a}\sin\frac{ak_i}{2} \equiv \hat{k}_i; \tag{48}$$

$$k_0 + 2\pi qT \longrightarrow \frac{2}{a}\sin a\frac{k_0 + 2\pi qT}{2} \equiv \hat{k}_0(q). \tag{49}$$

The lattice momentum varies inside the Brillouin zone: $-\pi/a < k_i < \pi/a$. The component k_0 is discrete and takes values: $2\pi Tn$, $n = 0, 1, \ldots, L_t - 1$.

The partition function for a 'charged' gluon normalized by the 'neutral' one is given by:

$$\ln\frac{Z_q}{Z_0} = -\frac{d-2}{2}\left[\ln\det(-\hat{k}_0(q)^2 - \textstyle\sum_i \hat{k}_i^2) - \ln\det(-\hat{k}_0^2 - \textstyle\sum_i \hat{k}_i^2)\right]. \tag{50}$$

We use the proper time trick to calculate (50). To simplify formulas we work in lattice units $a = 1$. The r.h.s. of (50) becomes:

$$\frac{d-2}{2}\frac{\mathcal{V}}{T}\sum_{k_0}\int_{-\pi}^{\pi}\prod_i\frac{dk_i}{2\pi}\int_0^\infty\frac{dt}{t}\Big[\exp\{-(\hat{k}_0(q)^2 + \textstyle\sum_i\hat{k}_i^2)t\} - \exp\{-(\hat{k}_0^2 + \textstyle\sum_i\hat{k}_i^2)t\}\Big] \tag{51}$$

To rewrite the sum over $k_0 = 0, 2\pi/L_t, \ldots, 2\pi(1 - 1/L_t)$ (remember that $T = 1/L_t$ in our units) we use the Poisson summation formula, which for a function $f(k_0)$ periodic with a period 2π has the form:

$$\sum_{k_0=0}^{2\pi(1-1/L_t)} f(k_0) = \sum_{\nu=-\infty}^{\infty}\int_{-\pi}^{\pi}\frac{dk_0}{2\pi}e^{iL_t\nu k_0}f(k_0). \tag{52}$$

We substitute (52) into (51), shift the variable k_0 and obtain for $\ln Z_q/Z_0$:

$$\frac{d-2}{2}\frac{\mathcal{V}}{T}\sum_{\nu=-\infty}^{\infty}\int_{-\pi}^{\pi}\prod_\mu\frac{dk_\mu}{2\pi}\int_0^\infty\frac{dt}{t}\Big[\exp\{-(\hat{k}_0^2 + iL_t\nu k_0 - i2\pi q\nu + \textstyle\sum_i\hat{k}_i^2)t\} - \exp\{-(\hat{k}_0^2 + iL_t\nu k_0 + \textstyle\sum_i\hat{k}_i^2)\}\Big]. \tag{53}$$

Integration over k_μ produces modified Bessel functions:

$$I_n(2t) = \int_{-\pi}^{\pi} \frac{dk}{2\pi} \exp\{2t\cos k + ink\}, \tag{54}$$

and t can be rescaled after that. Finally, we obtain the expression which replaces $V(q)$, eq. (36), at finite L_t:

$$V_{\rm lat}(q) = 2(N-1)(d-2)L_t^d \int_0^\infty \frac{dt}{t} \sum_{\nu=1}^{\infty} e^{-dt} I_{\nu L_t}(t)[I_0(t)]^{d-1}(1-\cos 2\pi q\nu) \tag{55}$$

It is instructive to see how the continuum limit $L_t \to \infty$ (i.e., $aT \to 0$) is recovered. For large n and large $t \gtrsim n$ the Bessel function behaves as:

$$e^{-t} I_n(t) \approx \frac{1}{\sqrt{2\pi t}} \exp\{-\frac{n^2}{2t}\} \quad \text{and} \quad e^{-t} I_0(t) \approx \frac{1}{\sqrt{2\pi t}}. \tag{56}$$

Only large t of order $(\nu L_t)^2$ will contribute to the integral in (55). After rescaling t by $(\nu L_t)^2$ and integrating we get the same expression as in (36).

The variation of q with z can be also taken into account. The gradient term on the lattice becomes:

$$\frac{\gamma^2}{2}(q(z+1) - q(z))^2, \tag{57}$$

so that the profile equation (39) is replaced with:

$$q(z+1) = q(z) + \sqrt{\frac{2}{\gamma^2} V_{\rm lat}(q)}, \tag{58}$$

where similarly to the continuum case

$$\gamma^2 = 8\pi^2 \frac{N-1}{N} \frac{T^{2-d}}{g^2} = 4\pi^2 \frac{N-1}{N^2} \beta L_t^{d-2}. \tag{59}$$

The interface tension is given by an expression similar to (40) except for α_0 being replaced by its lattice version:

$$\alpha = 4\pi \sqrt{\frac{N-1}{N}} \int_0^1 dq \sqrt{V_{\rm lat}(q)} \quad . \tag{60}$$

5 Action density profiles

An important quantity that we measure on the lattice is the expectation value of the plaquette action. In the continuum limit this corresponds to $\langle \boldsymbol{E}^2 + \boldsymbol{B}^2 \rangle$, where the Euclidean $\boldsymbol{E}$ is:

$$\boldsymbol{E} = -\partial_0 \boldsymbol{A} - \boldsymbol{D} A_0. \tag{61}$$

We also measure separately the expectation values of the plaquettes of each orientation, which correspond to $\langle E_y^2 \rangle$, $\langle E_z^2 \rangle$, $\langle B^2 \rangle$ in our $d = 3$ case.

An interesting result that we find in our Monte Carlo study is that these expectation values display nontrivial profiles, correlated with the position of the domain wall. One expects that at high T a perturbative calculation of these quantities is possible. In this section we perform such a calculation.[4]

We start again with the partition function (25) on a constant background $\underline{A}_0$. At high T the effective interaction is weak and we apply a saddle point approximation. We write:

$$Z(\underline{A}) = \int \mathcal{D}A_\mu \exp\left\{ -\frac{1}{2g^2} \int_0^{1/T} dt \int_{\boldsymbol{x}} (\boldsymbol{E}^2 + \boldsymbol{B}^2) \right\}, \tag{62}$$

where we linearize E and B:

$$\boldsymbol{E} = -\partial_0 \boldsymbol{A} - i[\underline{A}_0, \boldsymbol{A}] - \boldsymbol{\nabla} A_0; \qquad \boldsymbol{B} = \boldsymbol{\nabla} \times \boldsymbol{A}. \tag{63}$$

We have already calculated the integral (62) in Section 3:

$$Z(\underline{A}) \equiv Z(q) = \exp\left\{ -T^{d-1} \int_{\boldsymbol{x}} (V(q) - c) \right\}. \tag{64}$$

Now, to find the action density profiles we want to calculate things like $\langle \boldsymbol{E}^2 \rangle$ and $\langle \boldsymbol{B}^2 \rangle$, where the average is understood in terms of the probability distribution given by the integrand in (62). These averages depend on $\underline{A}$, or q. The easiest way to calculate $\langle \boldsymbol{E}^2 \rangle$ is to introduce a parameter, say ϵ, in front of this term in the exponent, do the integral and differentiate the logarithm of the result over ϵ. We shall do this shortly, but before that let us improve a bit on the formula (64). What we need to include

[4] Such profiles were also measured in [20]. Here, we show that at high T one can actually calculate them analytically.

is the contribution of zero point energies of the modes of the fields A. This contribution does not depend on the temperature and is not present in (64), but it gives an overwhelmingly dominant contribution to $\langle \boldsymbol{E}^2 \rangle$ and $\langle \boldsymbol{B}^2 \rangle$. Indeed, this contribution is of order $(1/a)^d$, where a is the lattice spacing (the UV cutoff), and is much larger than T^d - the thermal contribution. To see what we are missing consider calculating $\langle \boldsymbol{E}^2 + \boldsymbol{B}^2 \rangle$ from (64). For that one needs only to differentiate (the logarithm of) the right hand side over $(1/g^2)$. But the right hand side does not depend on g! This means that the quantity $\langle \boldsymbol{E}^2 + \boldsymbol{B}^2 \rangle$ (which is obviously not zero) gives the sum of zero point energies and has no thermal contribution at that order. To make this fact explicit imagine rescaling g^2 in (64) by a factor $1/\epsilon$. One can absorb this factor by rescaling the fields A by $\sqrt{\epsilon}$. This will change the measure by a factor $(\sqrt{\epsilon})^{(N^2-1)(d-1)\mathcal{N}}$, where $\mathcal{N} = T^{-1}\mathcal{V}/a^d$ is the total number of the lattice sites. The number $(N^2-1)(d-1)\mathcal{N}$ is simply the number of non-zero modes, or non-zero eigenvalues of the matrix of the quadratic form in the exponent (62). Eventually we get instead of (64):

$$Z(q) = g^{(N^2-1)(d-1)\mathcal{N}} \exp\left\{-T^{d-1}\int_{\boldsymbol{x}} (V(q) - c)\right\}. \tag{65}$$

Using (65) we get for any T:

$$\frac{1}{2g^2}\langle \boldsymbol{E}^2 + \boldsymbol{B}^2 \rangle = \frac{(N^2-1)(d-1)}{2}\, a^{-d}. \tag{66}$$

It means that each space component of the vector $\boldsymbol{E}$ or the tensor $\boldsymbol{B}$ has the average at $T = 0$ (due to Euclidean invariance):

$$\frac{1}{2g^2}\langle E_x^2 \rangle = \frac{N^2-1}{d}\, a^{-d}. \tag{67}$$

This is the dominant contribution and should be compared to $\beta(1 - \mathrm{tr}U_P/N)$ per plaquette which we measure (in our case $N = 2$, $d = 3$). It is indeed equal to 1 in lattice units up to a small correction. Part of this correction is the thermal effect.

To calculate the thermal part of the action density, multiply only the term $\boldsymbol{E}^2$ in (62) by a factor ϵ. Then consider the following transformation: $t' = t/\sqrt{\epsilon}$, $A'_0 = A_0\sqrt{\epsilon}$, $T' = T\sqrt{\epsilon}$ and $g'^2 = g^2/\sqrt{\epsilon}$. In terms of new variables

the integral is the same up to a Jacobian factor and thus:

$$\begin{aligned} Z(q) &= \int DA_\mu \exp\left\{-\frac{1}{2g^2}\int_0^{1/T} dt \int_{\boldsymbol{x}} (\epsilon \boldsymbol{E}^2 + \boldsymbol{B}^2)\right\} \\ &= \left(\frac{g}{\epsilon^{1/d}}\right)^{(N^2-1)(d-1)\mathcal{N}} \exp\left\{-(\sqrt{\epsilon}T)^{d-1}\int_{\boldsymbol{x}} (V(q)-c)\right\} \end{aligned} \tag{68}$$

Therefore,

$$\frac{1}{2g^2}\langle \boldsymbol{E}^2\rangle = (d-1)\frac{N^2-1}{d}\, a^{-d} - \frac{d-1}{2}(c - V(q))T^d. \tag{69}$$

The $\boldsymbol{E}^2$ is a sum of $d-1$ components each contributing equally. Using (66) and (69) we get also:

$$\frac{1}{2g^2}\langle \boldsymbol{B}^2\rangle = \frac{(d-1)(d-2)}{2}\frac{N^2-1}{d}\, a^{-d} + \frac{d-1}{2}(c - V(q))T^d. \tag{70}$$

Note that while $(1/2g^2)\langle \boldsymbol{E}^2 + \boldsymbol{B}^2\rangle$ is totally due to the vacuum zero point energy, it is $(1/2g^2)\langle \boldsymbol{B}^2 - \boldsymbol{E}^2\rangle$ that contains the thermal energy. The vacuum term in this quantity cancels in $d = 4$, because there is the same number of $\boldsymbol{E}$ and $\boldsymbol{B}$ components.

So far we have neglected the variation of q with z. This can be easily corrected for. It contributes only to $\langle E_z^2\rangle$ the amount $(\gamma^2/2)(\partial_z q)^2 T^d$, which is equal to $V(q)T^d$ due to (39).

Finally, we write down expressions for the plaquette action densities in our case ($N = 2$, $d = 3$). We use lattice units: $a = 1$, in which $T = 1/L_t$, and β is given by (45):

$$\begin{aligned} \frac{1}{2g^2}\langle B^2\rangle &= 1 + (c - V(q))\frac{1}{L_t^3} + O(1/\beta); \\ \frac{1}{2g^2}\langle E_y^2\rangle &= 1 - \frac{1}{2}(c - V(q))\frac{1}{L_t^3} + O(1/\beta); \\ \frac{1}{2g^2}\langle E_z^2\rangle &= 1 - \frac{1}{2}(c - 3V(q))\frac{1}{L_t^3} + O(1/\beta). \end{aligned} \tag{71}$$

The corrections of order $1/\beta$ are due to non-quadratic terms and are beyond our approximation. However, they should be the same for all plaquettes at

that order. They cancel in, e.g.: $\langle B^2\rangle - \langle E_y^2\rangle$ or $\langle B^2\rangle(q) - \langle B^2\rangle(0)$. The formulas (71) are in good agreement with our MC data (see Section 7).

What do we learn from all this? One can see, for example, that the thermal part in the fluctuations of $\langle B^2\rangle$ becomes negative at some q near $1/2$, i.e., inside the wall. This means that the $\langle B^2\rangle$ becomes smaller than the contribution of the vacuum fluctuations to that quantity![5] This is just another side of the old puzzle with negative entropy and thermal energy density [4, 9].

6 Finite size corrections

6.1 Roughening

Due to the long wavelength thermal fluctuations of its shape, an interface in 3 spatial dimensions oscillates from its central position by a distance which grows as the logarithm of its area. This roughening also occurs in 2 dimensions, where the effect is proportional to $\sqrt{L}_y$. Here we calculate the effect of the roughening on our measurements of the profile of the wall and the interface tension and show that this effect is rather small.

The roughening is due to long wavelength fluctuations of the shape of the interface. These fluctuations are therefore essentially classical: $\omega_k \ll T$. We can consider our interface in 2 spatial dimensions as a classical string of length L_y with tension and mass per unit length equal to σ. The string is a set of free oscillators, the normal modes. The amplitudes f_k of these are the Fourier components of $f(y)$, the shape of the string at a given instance. Each oscillator (mode) has energy T in the heat bath (equipartition). On the other hand, the mean energy of such an oscillator is $\sigma\omega_k^2\langle f_k^2\rangle$. The mean square of the fluctuation of the string is then:

$$\langle \int_0^{L_y} dy f^2(y)\rangle = \langle \sum_k f_k^2\rangle = \sum_k \frac{T}{\sigma\omega_k^2} \tag{72}$$

The dispersion law is: $\omega_k = k$. If we take $L_y = \infty$ and replace the sum with an integral it will diverge linearly: the soft modes get out of hand if L_y does not cut them off. For finite L_y the values of momenta q are given by the

[5] In other words, $\langle B^2\rangle - \langle E_y^2\rangle$ becomes negative.

periodic b.c.:

$$k = \frac{2\pi}{L} n, \quad n = 1, 2, 3, \ldots, \tag{73}$$

where $k = 0$ (translational mode) is removed by our procedure of shifting the center of the interface. In principle, our string approximation will break down at some large $k_{\max}$, but the value of this UV cutoff is not essential for the long wavelength effect we are interested in. We put $k_{\max} = \infty$. Thus we have:

$$\langle f^2(y) \rangle = \frac{2}{L_y} \sum_{n=1}^{\infty} \frac{T}{\sigma} \frac{L_y^2}{(2\pi n)^2}. \tag{74}$$

The factor of 2 is because for each n there is a cosine and a sine mode. The sum over n can be evaluated and we get for the mean square deviation of the wall from a straight line:

$$\Delta w^2 = \langle f^2(y) \rangle = \frac{T}{\sigma} \frac{L_y}{12}. \tag{75}$$

Let us estimate this effect in our case. Take, for example, $L_t = 3$ and $\beta = 75$:

$$\Delta w = \left(\frac{2}{\alpha} \sqrt{\frac{L_t^3}{\beta}} \frac{L_y}{12} \right)^{1/2} \approx \sqrt{L_y/50}, \tag{76}$$

where we used the formula (40) for σ and the relation (45). For $L_y = 12 - 60$ this varies from 0.5 to 1 or so, as compared to $w \sim 17$. We observe a slight variation of the width of the wall of roughly this size in our MC data, although it is no doubt optimistic to be applying a string formalism in a situation where the length of the wall is comparable to its width!

We conclude that roughening does not affect our estimates of the profile of the wall. This effect is small, because the wall is stiff, and L_y is not too large. So what we measure numerically is really the intrinsic profile of the interface.

One can also calculate the correction to the interface tension from the string-like fluctuations of the interface using the same idea that the string is a set of oscillators in a heat bath. A difficulty lies in the fact that unlike $\langle f^2 \rangle$ which is a convergent sum of $\langle f_k^2 \rangle$, the amplitudes of the oscillators, the sum of their free energies, $-T \ln(T/\omega_k) + \text{const}$, is divergent. This divergence is ultraviolet, however, and can be subtracted when computing the finite size dependence, similarly to the Casimir effect.

Another, more illuminating way of deriving this correction is to consider the $\mathcal{F}(q)$ in (37) as an effective potential energy for the long wavelength classical thermal fluctuations of the wall. The profile $q_0(z)$ satisfying (39) is a minimum of $\mathcal{F}(q)$ for the corresponding boundary conditions. The leading exponential behavior of the partition function is then:

$$Z_{\rm wall} \sim \exp\left\{-\frac{1}{T}\int_{\boldsymbol{x}}[\,\mathcal{F}(q_0(\boldsymbol{x}))-\mathcal{F}(0)\,]\right\} = \exp\left\{-\frac{\sigma L_y}{T}\right\}, \qquad (77)$$

where we subtracted the bulk free energy.

The pre-exponential correction to (77) is due to fluctuations of $q(y,z)$ around $q_0(z)$ and is given by the determinant:

$$\det{}'(-\gamma^2\boldsymbol{\nabla}^2 + V''(q_0(z)))^{-1/2}, \qquad (78)$$

where the prime on 'det' denotes the fact that we omitted the translational mode. This mode is proportional to $\partial_z q_0$. Properly normalized it produces a factor $\sqrt{\sigma L_y/\gamma^2 T}$ and an integration over the position of the center. The spectrum of the operator in (78) can be written as

$$\lambda = \gamma^2 k^2 + \lambda_m \qquad (79)$$

where $k = 2\pi n/L_y$ and λ_m are the eigenvalues of $-\gamma^2\partial_z^2 + V''(q_0(z))$. The $\lambda = \gamma^2 k^2$ band attached to the zero eigenvalue $\lambda_m = 0$, corresponds to fluctuations of the wall as a whole. The roughening effects are due to these gapless fluctuations. The corresponding determinant is $\det{}'(-\gamma^2\partial_y^2)$. We can regularize it in the UV by dividing it by a similar determinant with $L_y = \infty$. On dimensional grounds:

$$\frac{\det{}'(-\gamma^2\partial_y^2)_{L_y}}{\det(-\gamma^2\partial_y^2)_\infty} = \frac{L_y^2}{\gamma^2}\cdot{\rm const}, \qquad (80)$$

Other eigenvalues are not related to the roughening and we neglect their contribution in our estimate. Collecting all the factors we obtain:

$$Z_{\rm wall} \approx {\rm const}\int dz\,\sqrt{\frac{\sigma}{TL_y}}\exp\left\{-\frac{\sigma L_y}{T}\right\} = {\rm const}\,\sqrt{\frac{\sigma L_z^2}{TL_y}}\exp\left\{-\frac{\sigma L_y}{T}\right\}. \qquad (81)$$

From (81) we can read off the correction to the interface tension[6]:

$$\Delta\sigma = \frac{T}{2L_y} \ln \frac{TL_y}{\sigma L_z^2} + O(T/L_y) \tag{82}$$

This means that the correction to α, in the way we measure it in our simulations (see Section 7), is given by:

$$\Delta\alpha = \frac{4L_t^{3/2}}{L_y}\sqrt{\beta}\frac{\partial}{\partial\beta}\left(\frac{\Delta\sigma L_y}{T}\right) \approx -\frac{L_t^{3/2}}{L_y\sqrt{\beta}}. \tag{83}$$

For example, at $\beta = 75$, $L_t = 3$ and $L_y \sim 50$ this correction is only about 0.2%.

6.2 Finite L_z corrections

In the previous section we discussed the roughening effect which introduces corrections of the type $(\ln L_y)/L_y$ to σ. In this section we discuss another source of finite size effects: the finiteness of L_z. There are two ways the finiteness of L_z affects the free energy of the wall. First, there is a correction to $V(q)$ itself because it is given by one-loop integrals which depend on L_z through the quantization of momenta running in the loop.[7] This correction should be of order $(T/L_z)^2$ and is relatively small. For $L_z \gtrsim w$ this correction is beyond our leading order in g approximation, because $(T/w)^2$ is of order g^2.

The second source of corrections is due to the finiteness of L_z/w. It is obtained by calculating the action of a particle with a 'mass' γ^2 which, moving in the potential $-V(q)$, returns to its starting value of q in a period of 'time' $2L_z$ This finite size effect we estimate here and show that, for large enough L_z, it is exponential in $d > 3$, i.e., $\exp\{-L_z/w\}$, and Gaussian in $d = 3$, i.e., $\exp\{-L_z^2/w^2\}$.

So we consider a trajectory which starts at rest at $q = \varepsilon$ and arrives at $q = 1 - \varepsilon$ precisely after a given 'time' L_z so as to satisfy the boundary

[6]This correction is analogous to the Luscher's correction [21], but for a classical string in a thermal bath, rather than a strip (quantum string at $T = 0$). The universal coefficient of the Coulomb correction $1/L$ to the free energy in Luscher's case becomes in our case the coefficient of the $\ln L$ correction. It is especially obvious in the interpretation given by Stack and Stone [22].

[7]There is, of course, a similar dependence on L_y.

condition on the Polyakov loop. The trajectory satisfies a Lagrange-Euler equation which can be integrated to give ('energy' conservation):

$$\frac{\gamma^2}{2}(q')^2 - V(q) = -V(\varepsilon) \equiv E. \tag{84}$$

We can use it to relate L_z to ε:

$$L_z(\varepsilon) = \int_\varepsilon^{1-\varepsilon} \frac{dq}{\sqrt{\frac{2}{\gamma^2}(V(q) - V(\varepsilon))}} \tag{85}$$

The action can be cast into the form:

$$S(\varepsilon) = \int_0^{L_z} dz\,[\frac{\gamma^2}{2}(q')^2 + V(q)] = \int_\varepsilon^{1-\varepsilon} dq\,\sqrt{2\gamma^2(V(q) - V(\varepsilon))} + V(\varepsilon)L_z(\varepsilon), \tag{86}$$

which is convenient for the numerical evaluation of $S(\varepsilon)$. Also note, that this form is familiar in theoretical mechanics as $dS = pdq - Edt$. The equations (85) and (86) give a parametric representation of S as a function of L_z which we use to evaluate the correction numerically.

To find the asymptotic dependence of S on L_z one can use the relation:

$$\frac{dS}{dL_z} = V(\varepsilon), \tag{87}$$

which is a consequence of $dS = pdq - Edt$, and can be also derived explicitly from (85), (86).

Now we use the asymptotic form of $V(q)$ at small q. For $d > 3$ it is:

$$V(q) = bq^2 + O(q^4) \quad (d > 3), \tag{88}$$

where b is a constant which depends on N and d (96). Using this form we get from (85):

$$L_z(\varepsilon) = 2\sqrt{\frac{\gamma^2}{2b}} \ln\frac{1}{\varepsilon} + O(1), \quad (d > 3). \tag{89}$$

Integrating the equation:

$$\frac{dS}{dL_z} = b\varepsilon^2 + O(\varepsilon^4) \approx \text{ const } b \exp\left\{-\sqrt{\frac{2b}{\gamma^2}} L_z\right\}, \quad (d > 3), \tag{90}$$

we obtain the asymptotic form of the large L_z correction to S:

$$\delta S \sim -\text{ const } \sqrt{\frac{b\gamma^2}{2}} \exp\left\{-\sqrt{\frac{2b}{\gamma^2}} L_z\right\}, \quad (d>3). \tag{91}$$

For $d=3$, however, we have:

$$V(q) = bq^2 \ln\frac{1}{q} + O(q^2), \quad (d=3). \tag{92}$$

where b is given by (97). This leads to

$$L_z(\varepsilon) = \sqrt{\frac{8\gamma^2}{b}} \sqrt{\ln\frac{1}{\varepsilon}} + O(1), \quad (d=3); \tag{93}$$

and

$$\frac{dS}{dL_z} \approx \text{ const } \frac{b^2 L_z^2}{8\gamma^2} \exp\{-\frac{bL_z^2}{4\gamma^2}\}, \quad (d=3); \tag{94}$$

Integrating we obtain:

$$\delta S \sim -\text{ const } \frac{bL_z}{4} \exp\{-\frac{b}{4\gamma^2} L_z^2\}, \quad (d=3). \tag{95}$$

We see that the asymptotic form of the correction is related to the way the tail of the wall decays: exponential in $d>3$ and Gaussian in $d=3$.[8]

From (36) we find for b in (88):

$$b = (2\pi)^2 (N-1)(d-2) \frac{\Gamma(d/2)}{\pi^{d/2}} \zeta(d-2), \quad (d>3); \tag{96}$$

while in $d=3$ the value of b defined as in (92) equals:

$$b = 2\pi(N-1), \quad (d=3). \tag{97}$$

To get an idea of the size of this correction in our case let us estimate it for the case of $\beta = 100$, $L_t = 4$, $L_z = 120$. We get $\gamma^2 = \pi^2 \beta L_t = 400\pi^2 \approx 60^2$. The exponent is $bL_z^2/4\gamma^2 \approx (L_z/50)^2 \approx 5.8$ and $e^{-5.8} \approx 1/300$. The pre-exponent $bL_z/4 \approx 200$. Thus $\delta S \sim 1$. This should be compared to:

$$S_0 = \int_0^1 dq \sqrt{2\gamma^2 V(q)} \approx 50. \tag{98}$$

Thus the correction, $\delta S/S_0$, is of the order of a (few) percent. In the following section we shall evaluate these corrections, numerically, for all L_z and not just large L_z as herein.

[8] See, however, footnote 2 on page 18 and the related discussion.

7 Numerical Simulations of Domain Walls

As we have seen, at high temperatures the theory appears to have degenerate vacua which are separated by domain walls. At asymptotic temperatures many properties of these domain walls can be calculated in perturbation theory; indeed the existence of these interfaces can only be seen when one goes beyond tree level. However, as we remarked earlier, the presence of infrared divergences in higher-orders has raised doubts about the applicability of perturbation theory and, indeed, about the actual existence of the interface. To address these doubts we have performed accurate computer simulations of the domain walls, and have compared what we find with the results of the perturbative calculations. These computer simulations will be described in this section.

If we simulate the high temperature $SU(2)$ gauge theory in a finite but large spatial volume, with periodic boundary conditions, then we expect some fraction of the field configurations to contain both $Z(2)$ phases in different portions of the torus. Such a configuration will contain domain walls separating the two phases and in principle one could study the domain walls by focusing on these particular field configurations. However the relative probability of such configurations is very small for the temperatures of interest and they would not be encountered in a typical Monte Carlo calculation. So we have to use an alternative less direct method. What we do is to impose twisted boundary conditions on our system, so enforcing the existence of at least one domain wall. This will be described in Section 7.1. In Section 7.2 we show how the domain wall can be interpreted as a 't Hooft disorder loop. We then specify the physical quantities that we plan to calculate and describe the methods by which we do so in Section 7.3. Section 7.4 summarises our Monte Carlo results. Of course, it is crucial to demonstrate that we have all finite-volume effects under control — after all, it is infrared effects that are the potential problem here — and this we do in Section 7.5. Finally, in Section 7.6, we will take our raw 'data' and use it to extract quantities that are of direct physical interest in the present context and compare them to the perturbative predictions.

7.1 Twisted Boundary Conditions

We work on lattices of size $L_y \times L_z \times L_t$ in lattice units. The Euclidean time extent determines the temperature, $aT = 1/L_t$, of the field theory. The partition function contains the factor $\exp(-\beta S)$ where $\beta = 4/(ag^2)$ and the lattice action is as in (42):

$$S = \sum_p [1 - \frac{1}{2}\,\mathrm{tr}U_p], \tag{99}$$

where U_p is the path ordered product of the $SU(2)$ matrices, U_l, on the links, l, that form the boundary of the plaquette p.

The simplest and most usual way to introduce twisted boundary conditions is as follows [20]. We change the above action to a twisted action, S_{tw}, by replacing $\mathrm{tr}U_p$ with $-\mathrm{tr}U_p$ for those plaquettes in the zt plane that emanate from the sites (y, z, t) where z and t are fixed to some particular values, say $z = j$ and $t = k$, while y takes all values from 1 to L_y (see Fig. 1).

The system with this altered action and with periodic boundary conditions is equivalent to the system with the original action but with twisted boundary conditions [23]. This we see from the following argument. Firstly, let us choose labeling z of the sites so that $j = L_z$, i.e. the twist is between $z = L_z$ and $z = 1$. Secondly, to include the possibility of boundary conditions that are not periodic it is convenient to extend our labeling to include $z = 0$, as well as $z = 1, \ldots, L_z$. If the system is periodic then corresponding sites and links with $z = 0$ and $z = L_z$ are identified (and similarly for other directions). Then the system with a twisted action can be viewed as a system with the original action but with fields which are not periodic. To be more specific they are periodic except that for $y = 1, \ldots, L_y$ and $t = k$ the time-like link at $z = 0$ is mapped into the negative of itself at $z = L_z$. This is the lattice version of the twisted boundary conditions described in Section 2.1.

One can move the zt position of the line of twisted plaquettes by flipping the sign of all U_l which bound these plaquettes from one of the sides; but one cannot undo the twist completely. It should be clear that the position of the twist does not carry any physical significance since it can be moved by such a redefinition of the variables U_l.

How does the twist lead to the presence of a domain wall? To see this consider the same labeling of sites as we have just used. With free boundary conditions the system would spend most of the time in one of the two phases where Polyakov loops are all near $+1$ or all near -1. With the twisted boundary condition a Polyakov loop at $z = 0$ is mapped onto negative of itself at $z = L_z$. Therefore a homogeneous configuration is frustrated and the Polyakov loops must create a nontrivial profile in the z direction to interpolate between $z = 0$ and $z = L_z$.

So to study the high T properties of domain walls we perform Monte Carlo calculations on lattices with periodic boundary conditions but with a twisted action. How well defined is the domain wall in practice? To answer this question we show in Fig. 2a the distribution of Polyakov loops on a typical field configuration taken from a $30 \times 80 \times 2$ lattice at $\beta = 100$. In physical units this corresponds to a temperature $T \sim 30T_c$ where T_c is the deconfining temperature. We see that the domain wall is very well defined, with relatively small fluctuations around a smooth background distribution. This is in fact the highest value of T at which we work. The lowest value is on a $12 \times 30 \times 2$ lattice at $\beta = 7$ corresponding to $T \sim 2T_c$. There a typical field configuration looks as in Fig. 2b. The fluctuations are now much larger, but the domain wall can still be unambiguously located. So it is clear that, for the range of T we study, there is no ambiguity in identifying the domain wall.

7.2 Domain Walls as Disorder Loops

Before going on to the details of the calculations, we address the following natural question. Since the twist is entirely symmetric in z and t why should the 'domain wall' separate regions in z rather than regions in t? This question can be plausibly answered, in a way that highlights the physics, by first considering the twisted system at very low T where the system is manifestly rotationally invariant. Here introducing a twist introduces into the system a 't Hooft disorder loop [24] which is closed through the boundary in the y-direction. This loop will presumably be a flux tube whose width will be on the order of the characteristic length scale of the theory, which here is $1/g^2$. Its special property is that it if one considers the gauge potential on a closed path that encircles the disorder loop far from its centre, then the presence of this loop leads to the potential acquiring a gauge transformation that goes

from 1 to a non-trivial element of the centre as we go once around this closed path. So if we take a large Wilson loop and pierce it once (or an odd number of times) by this disorder loop, then the value of the Wilson loop is changed by a factor of -1 as compared to the value it would possess in the absence of the disorder loop. Hence the name 'disorder loop'. It is clear that if the vacuum contained a condensate of such loops, then these would be sufficient to ensure that large Wilson loops varied as the exponential of their area, so that we had linear confinement. Suppose we now increase T by reducing the extent of the system in the t-direction. Clearly at some point the time extent will become smaller than the width of the flux tube, the tube will become squeezed so that it extends right across the time direction while still extending over a finite region in the z-direction. This will occur once T is sufficiently large compared to g^2; presumably around the deconfining transition. So at high temperatures our 'domain wall' is actually a squeezed disorder loop that closes upon itself through the y-direction. It is indeed symmetric in z and t except for the deformation induced by the limited t extent. The fact that the Polyakov loops on either side of the wall have opposite signs is what one might expect from such a squeezed 't Hooft disorder loop.

We have simplified the above argument by assuming that the disorder loops exist as definite field fluctuations in the low-T theory. This is assuming a great deal of course. Whether they do so exist is one of the central questions in the still unresolved problem of colour confinement. This makes the connection between these loops and the domain walls at high-T of added interest.

7.3 Quantities Calculated

We perform calculations on lattices with and without a twist. The simplest and most interesting quantity we extract is the extra action, S_w, associated with the presence of a domain wall. If both twisted and untwisted lattices are of the same size, then

$$S_w = \langle S_{\rm tw} \rangle - \langle S_{\rm nt} \rangle \tag{100}$$

where $\langle S_{\rm tw} \rangle$, $\langle S_{\rm nt} \rangle$ are the average values of the twisted and untwisted actions, as defined in Section 7.1. The extra action is related to the free energy of

the wall, $F_w \equiv F_{\rm tw} - F_{\rm nt}$, by

$$\frac{\partial}{\partial\beta}\left(\frac{F_w}{T}\right) = S_w \tag{101}$$

where the derivative is taken at constant values of L_y, L_z, L_t. Using this relationship we shall test the one-loop prediction for F_w.

It might appear that changing the action for a line of L_y parallel plaquettes could introduce some additional *local* contribution to $\langle S_{\rm tw}\rangle - \langle S_{\rm nt}\rangle$ which is not related to the free energy of the wall. That this is not so one can see by considering a system with 2 parallel twists. This system is equivalent to a system without a twist after a redefinition of variables U_l which move the twists to a single position where they cancel each other.

In addition to making predictions for the domain wall free energy, perturbation theory can also be used to predict the detailed shape of the domain wall as it interpolates between the two $Z(N)$ vacua. In the Monte Carlo calculations the domain wall is free to move and so if we are to obtain an average profile, we need to shift our origin, in each Monte Carlo generated configuration, to the centre of the domain wall. We also need to take into account the presence of the twist, since the Polyakov loops change sign as one moves through it. Our algorithm is as follows. Consider a single Monte Carlo generated field configuration. First we average Polyakov loops over y. We write this average as $p(z)$. We now want to identify the location, $z = z_c$, of the centre of the domain wall. This is defined operationally as follows. We first identify the values of z where $p(z)$ changes from positive to negative values (factoring out, of course, the trivial change at the twist itself). Clearly the number of such changes must be odd. In practice the domain wall is very smooth at high T — as one can see in Fig. 2 — and it is almost always the case that there is only one place where there is a sign change. This occurs between sites and we shift our origin in z so that the sites where the sign changes are labeled by $z = 0$ and $z = 1$. We now ensure that $p(z = 1) > 0$ by multiplying the whole profile by -1, if necessary. Our range of z is now from $-L_z/2 + 1$ to $+L_z/2$. Somewhere in this range there is the twist and the value of $p(z)$ will flip sign there. If this occurs for $z \geq 1$ then we flip the signs of $p(z)$ for values of z beyond the twist; if it occurs for $z \leq 0$ then we flip the signs for z before the twist. In this way we obtain a wall profile with $p(z \geq 1) > 0$ and $p(z \leq 0) < 0$. We can now average this profile over many configurations to obtain an average profile. This will be symmetric about

$z = 1/2$ so we can fold the profile over (with a sign flip) so that it is defined for $1 \leq z \leq L_z/2$ and is positive. This is our final averaged profile. Note that in any individual configuration the centre of the domain wall may be closer to $z = 0$ than to $z = 1$. That is to say, our profile is 'smeared' over distances $\delta z \sim 1/2$.

In rare cases a given configuration contains more than one sign change in $p(z)$ (always factoring out the trivial sign change at the twist). The number of these sign changes is clearly odd. There are two possibilities. One is that we have a configuration with more than one domain wall, i.e. the one enforced by the twist plus pairs that are genuine quantum fluctuations. In this case we would typically expect at least one large gap in z between the walls. The more trivial possibility is that we might be simply seeing a large fluctuation of the values of $p(z)$ near the centre of the wall (where the values are small on the average). This would be characterised by very small gaps between the locations of the sign changes. The first type of configuration, which we should not include in our average, did not occur in any of the calculations that we include below. (It does occur if we approach the deconfining transition or if we make the extent in y of the lattice, and hence of the wall, sufficiently small.) The second type of configuration we should include and we do so by taking its centre to be located in the middle sign change. In practice these configurations are so rare that there is no visible change in any extracted quantities whether we include them or not.

Having obtained a centre for the wall from the Polyakov loop distribution, we can also define an action profile for the wall, and we can clearly do this separately for the different $\mu\nu$ components of the action.

A quite different but equally interesting quantity is the electric screening mass, m_D. This can be obtained from the lightest mass, m_P, that couples to Polyakov loops, and hence from the tail of the wall profile. We expect that for large enough z,

$$p(\infty) - p(z) \propto e^{-am_P z} \tag{102}$$

where $p(\infty)$ can be obtained either by working with very large lattices, or by performing simulations on a lattice without a twist and using the average value of the Polyakov loop obtained therein. So if we define an effective mass by

$$am_{\rm eff}(z) = \ln \frac{p(\infty) - p(z-1)}{p(\infty) - p(z)} \tag{103}$$

then

$$am_P = \lim_{z\to\infty} am_{\rm eff}(z) \tag{104}$$

In practice we would extract m_P from $m_{\rm eff}$ once we were at large enough z that the latter had become independent of z. The electric screening mass, m_D, should then be given by $m_P = 2m_D$ (see below).

On a finite lattice the above needs to be altered because we expect contributions going both ways around the z-torus. So instead of (102) we use

$$p(\infty) - p(z) \propto e^{-am_P z} + e^{-am_P(L_z - z)} \tag{105}$$

and alter (103) correspondingly.

Since we need to calculate the average action without a twist, we can also calculate the screening mass on these untwisted field configurations. Here we follow standard techniques for such mass calculations [25]. We construct $p_y = 0$ sums of Polyakov loops at each value of z and then obtain the vacuum-subtracted correlation function, $C(z_1 - z_2)$, as a function of their separation, $z = z_1 - z_2$. For large separation z we have $C(z) \propto \exp(-am_P z)$. We define an effective mass $am_{\rm eff}(z) = \ln[C(z-1)/C(z)]$, and we increase z until $m_{\rm eff}$ becomes independent of z. At this point we can estimate $m_P = m_{\rm eff}$. This calculation has the advantage that we can prove that $m_{\rm eff}(z) \geq m_{\rm eff}(\infty)$. In practice we modify this formalism for the periodicity in z as described above. In addition we calculate with a range of smeared Polyakov loops and use the correlation function that minimizes $m_{\rm eff}(z = 1)$; in the spirit of a variational calculation. However, this turns out not to be really necessary here; unlike the situation at $T = 0$. As we shall see below, this method turns out to be much more efficient for the calculation of screening masses than using the tails of domain walls.

7.4 Monte Carlo simulations

Our Monte Carlo simulations were performed on a variety of periodic lattices with and without a twist. We used a standard heat-bath update algorithm mixed with over-relaxation steps.

The control of finite volume effects is particularly important in these calculations since it is infra-red effects that are usually seen as being at the root of any possible breakdown of perturbation theory at high temperatures. We have therefore performed extensive numerical checks of finite volume effects

and these will be described in detail in Section 7.5. In this section we shall confine ourselves to a presentation of those results that have been obtained on lattices which are sufficiently large that any finite-volume corrections are much smaller than our (very small) statistical errors. This will, of course, need to be demonstrated and we shall do so later.

Now, let us estimate how large the required volumes must be in lattice units. If we use a periodic $L_y \times L_z \times L_t$ lattice, this corresponds to the fields in the spatial $L_y \times L_z$ volume being at a temperature $aT = 1/L_t$. The dimensionless inverse coupling β, as we have seen, is related to the dimensionful coupling, g^2 by $\beta = 4/ag^2$. Thus in physical units the temperature is $T/g^2 = \beta/4L_t$, and, at a fixed value of L_t, $\beta \propto T$. Perturbation theory is expected to be most reliable at very high T, so we want to study the theory for very large β. The characteristic length scale at high T is of the order of $1/gT^{1/2}$: the inverse of the Debye mass $1/m_D$ and the width of the wall w are of that order. Therefore the spatial sizes in units of a must satisfy:

$$L_y, L_z \gg \frac{1}{ag\sqrt{T}} = L_t\sqrt{\frac{T}{g^2}} \tag{106}$$

From (106) we see that for a fixed value of the temperature in physical units, T/g^2, the required volumes will be smallest, in lattice units, for $L_t = 2$ (since $L_t = 1$ is not sensible). Since the perturbative properties of the domain wall can be calculated on the lattice, the minimal calculation one might perform is to do everything at $L_t = 2$. However in this case a is as large as possible in units of $1/T$ ($aT = 1/L_t = 1/2$) and since there have been suggestions [9] that high-T perturbation theory might break down as $a \to 0$ we choose to perform calculations for several values of L_t. (This will have other advantages that will become apparent below.) We shall cover a range of temperatures for $L_t = 2, 3, 4$ and we shall perform a calculation at one reasonably high value of T for the case $L_t = 6$. In this latter case $aT = 1/6$ which is surely small enough that any breakdown of perturbation theory, as $a \to 0$, should have become prominent.

In Table 1 we list the average values of the plaquette, $1 - s_{\rm nt} \equiv \frac{1}{2}\langle {\rm tr} U_p \rangle$, for the calculations without a twist. In Table 2 we do the same for the corresponding quantity, $1 - s_{\rm tw}$, with a twist. We show the values of β, the lattice sizes, the number of Monte Carlo sweeps and the average plaquette action. In the twisted case we perform 'measurements' every Monte Carlo sweep; in

the untwisted case every four sweeps. The typical number of thermalisation sweeps prior to taking any measurements is between 25000 and 50000. The errors, given in brackets, are typically based on 40 or 50 bins. In a few of the lower statistics cases we use as few as 25 bins. The reader will note that at some values of the parameters we have several different lattices. These arose during the finite volume studies that will be described in detail later on. The measurements that we list here are those that do not suffer significant finite-size corrections (and are statistically accurate enough to be useful). At the different values of L_t we have chosen values of β such that the temperatures, in units of g^2, are roughly the same, although for higher L_t we are forced to cover more limited ranges of T. (The reader may be puzzled that in some cases β has not been chosen exactly proportional to L_t; for the purposes of the work in this paper no particular significance should be attached to these choices.) If we now multiply $s_{\rm tw} - s_{\rm nt}$ by the number of plaquettes in the twisted lattice, which is the one containing the domain wall, we obtain a value for S_w and hence, from (101), information on F_w. We shall see later on what this comparison tells us about the accuracy of perturbation theory.

As described in the previous section, the lightest mass that couples to Polyakov loops, is of particular interest because it is related to the Debye screening mass. It can be calculated either from correlations of Polyakov loops in the system without a twist, or from the way the tail of the domain wall merges into the vacuum once we are far enough away from the centre of the wall. In Fig. 3 we show the effective masses as obtained by the two methods. In Fig. 3a we have chosen our highest value of T for $L_t = 3$ while in Fig. 3b we show what one obtains for a medium value of T with $L_t = 2$. We see that in both cases the values of $am_{\rm eff}(z)$ as obtained from Polyakov loop correlations do become independent of z at larger z, and that these 'plateaux' occur early enough for the errors to be very small. Since in this case $m_{\rm eff}(z)$ is always an upper bound on m_P, we can extract an accurate estimate of m_P using the first value of the effective mass that is, within errors, on the plateau. The effective masses obtained from the domain walls are clearly consistent with being asymptotic to these mass values. However it is equally clear that they would give us much less accurate estimates of m_P. (We would need to do fits with at least two masses, since there are no convenient plateaux, and so the errors on m_P would be perhaps an order of magnitude greater. Moreover the assumption that the effective masses asymptote from below, while reasonable, introduces a difficult to quantify

extra systematic error.) So from now on we shall only use the values of m_P as extracted from Polyakov loop correlations. These are listed in Table 3, for those lattice volumes which do not suffer significant finite-volume corrections.

To obtain the extra action of the domain wall, S_w, at a particular value of β, we take the difference $s_{\rm tw} - s_{\rm nt}$ at that β and multiply by the number of plaquettes on the twisted lattice, which contains the domain wall. We expect that this extra action will be proportional to the length of the domain wall, i.e. to L_y, as long as L_y is not very small. (This and the related question of roughening will be addressed when we discuss finite volume corrections.) So we form the quantity S_w/L_y, which is the extra action of the wall per unit length (in units of the lattice spacing). If we have values of this quantity for several values of L_y at a given value of β and L_t, we can average them to obtain our best overall estimate. In Table 4 we present our final averages for this quantity and for the mass am_P, as obtained by averaging the values given in Tables 1-3. These will form the basic raw material for our later comparisons with perturbation theory.

7.5 Finite Volume Corrections

We shall be using our values of S_w to test perturbation theory. The details of the T and L_t dependence will be important in this comparison. Since the size of the domain wall varies with T, it is important that we control any finite volume corrections at all values of our parameters. Otherwise part of the T dependence we observe might be due to such corrections. In this section we describe in detail how we control finite size effects. We begin with effects of finite L_z and then consider finite L_y.

To establish how the finite periodicity in the z-direction affects the action of the domain wall, we perform numerical calculations for a large range of values of L_z. Since these effects may well vary with the lattice spacing, i.e. with $aT = 1/L_t$, we perform such calculations for two different values of L_t, but at the same value of physical temperature T/g^2. Since the finite-size corrections may differ for the contributions that are leading and non-leading in g^2/T, we also perform the calculations for two different values of T/g^2 at the same value of L_t. The parameter values and the corresponding values of S_w/L_y are displayed in Table 5. As we discussed previously, see (106), the natural scale for the domain wall should be of the order of $1/agT^{1/2} = \sqrt{\beta L_t}/2$. This is the scale that appears in perturbation theory (38,59): $\gamma =$

$\pi\sqrt{\beta L_t}$. We therefore plot in Fig. 4 the values shown in Table 5 against the scaled lattice length L_z/γ. We see that to a good approximation the finite size effects are indeed just functions of this scaled length. We also see that the finite size effects vary from being very large to being very small over a narrow range of values of L_z/γ. Indeed, the domain wall effectively disappears for $L_z/\gamma \leq 0.8$, and while the corrections are still large for $L_z/\gamma \sim 0.9$ to 1.1, they have become invisible, within our statistical errors by the time $L_z/\gamma \sim 1.35$. We therefore see that the values in Tables 2-4, which all correspond to lattices satisfying $L_z/\gamma \geq 1.65$, are effectively for $L_z = \infty$. As a final precaution against the unexpected, we show in Table 6 some further calculations obtained for a wide range of values of β and T. Taking these together with the values in Tables 1-3 confirms that the pattern of finite size effects we see in Fig. 4 is indeed characteristic of the range of T and a covered by the calculations in this paper.

Since the finite size effects appear to be insensitive to the value of T, it is interesting to ask whether they can be reproduced in leading order perturbation theory, which, after all, is supposedly exact in the $T = \infty$ limit. The appropriate formalism is that of the 'ball rolling in the inverse potential' as described in Section 6. To that order the finite size effects are functions of the scaled length L_z/γ, as can be seen from eqs. (85,86). In Section 6.2 we solved the equations analytically in the limit of large L_z/γ. In this section we solve them numerically for all L_z/γ, and different L_t, using $V_{\rm lat}(q)$. We note that solution does not exist if the 'time' $2L_z$ after which the particle has to come back oscillating around $q = 1/2$ is smaller than the period of small harmonic oscillations around this point. This gives for the minimal value of L_z: $L_z/\gamma = \sqrt{\pi/4\ln 2} = 1.06$ (for $L_t = \infty$). This fits in well with what we observe in Fig. 4. For large L_z the correction is exponential in ${L_z}^2$ in this order. This would be difficult to see given our finite statistical errors. Moreover we know that in the full theory the correction must ultimately be exponential in L_z. From Fig. 4 we see that leading order perturbation theory describes the observed finite size effects reasonably well. We also see that our criterion, $L_z/\gamma \geq 1.65$, should be a safe one to use for all values of L_t.

We now turn to the finite-size effects associated with the transverse length of the domain wall, L_y. If L_y is small enough then extra domain walls will be produced as quantum fluctuations since the main factor in the suppression of domain wall excitation is $\sim \exp(-\beta S_w)$ and $S_w \propto L_y$. When L_y becomes

sufficiently large we expect the leading correction to be that due to roughening, as discussed in Section 6.1. As we see in (83) these corrections should be very small for the parameters we use. Of course at asymptotically large L_y the profile of the domain wall, defined by averaging the Polyakov loops over y, will broaden as $\sqrt{L_y}$. For our values of L_y the broadening of the profile is small (see Section 6.1).

To find out what are the corrections at finite L_y, we have performed calculations for a range of values of L_y. As in our study of the L_z dependence we do so for two values of L_t at the same value of T/g^2 and for two values of T at the same value of L_t. These are presented in Table 7. We see that the surface tension shows no variation with L_y at, say, the 2σ level except for $L_y = 4$ at $\beta = 25$. Here there appears to be a $\sim 4 - 8\%$ reduction in the tension. This compares well with (83) — recalling that $\alpha \sim 6$ for $L_t = 2$, although we should certainly not expect (83) to be accurate for such small L_y.

However, while we see that there are no significant L_y corrections to the surface tension, this is certainly not the case for the Polyakov loop mass, am_P. We see that not only does this mass gap show large finite size corrections for the smallest values of L_y, but that these corrections become noticeable for values of L_y that are not so small. In fact the pattern we see is consistent with a relative correction of the form $\sim \exp(-am_P L_y)$.

The extensive finite-size studies we have carried out in this section show that the potentially dangerous infra-red effects are in fact under control and that the values of the surface tension and mass gap that we shall be using in the next Section, may be regarded as having been obtained on an infinite system.

7.6 Surface Tension and Debye Screening Mass

Even without looking at the detailed numbers in our Tables, there are two properties of the domain walls that are immediately apparent. One is that the probability of such a wall being produced at high T is very small. The other is that the walls have a finite width. Do these qualitative features already teach us something?

Consider the finite width. This is significant because at tree level a wall would have infinite width. That is to say, the width of the wall would be $\propto L_z$ however large we made L_z. One can easily see this by considering the

minimum action configuration that interpolates between the vacuum with all Polyakov loops $+1$ and the vacuum with all loops -1. The fact that the walls we generate are of a finite width, i.e. independent of L_z once L_z is sufficiently large, is implicit in the finite volume studies of the previous section. However it is worth showing this explicitly. We define the width of the wall, $w(90\%)$, as the distance, in lattice units, from the value of z where the Polyakov loop is 90% of its asymptotic value to the point where it is of the same magnitude but of opposite sign. As a check that there is nothing special about the choice of 90%, we shall also define a width, $w(2/3)$, on the basis of 2/3 of the asymptotic value. In Fig. 5 we show how w varies with L_z in two of the cases where we have made measurements for a wide range of lattice lengths. What we see is that the width of the wall does not change with increasing L_z once $L_z > 2w(90\%)$: the wall does indeed have a finite fixed width.

How does this width depend on T? We extract w from all our large volume calculations (essentially those listed in Table 2) and plot the results against $\gamma = \pi(\beta L_t)^{1/2}$ in Fig. 6. This variable, as we have seen, determines the width of the wall in leading-order perturbation theory. As a matter of fact, $\gamma \approx w(0.97)$ to that order in the continuum limit,i.e. for $L_t = \infty$. We see from Fig. 6 that for each value of L_t the width varies linearly with γ, with significant deviations only at the very lowest values of T. The lines for different L_t are close to each other, but do not coincide. This is what one expects in perturbation theory; the width has to be proportional to the one scale, $\gamma = 2\pi/g\sqrt{T}$, but the constant of proportionality will suffer lattice spacing corrections, i.e. will depend on $aT \equiv 1/L_t$. We show in Fig. 6 the lines one gets in perturbation theory. Clearly these are consistent.

The corrections to perturbation theory are governed by $g^2/T = 4L_t/\beta$. We note that for $\beta = 7$ at $L_t = 2$, and for the corresponding values of β at other values of L_t, this is ≥ 1. It is therefore remarkable that the calculated widths deviate by no more than $\sim 10\%$ from the leading-order perturbative high T expectations. It would seem that not only does perturbation theory work well where we might expect it to, but it even works well where we have little reason to hope it might. We shall see other instances of this later on.

The fact that wall-like quantum fluctuations are very rare tells us that the action a wall costs is positive: $S_w > 0$. Using (101) and noting that, for fixed L_t and L_y, $\partial/\partial\beta \sim \partial/\partial T$ because $\beta \equiv 4/ag^2 = 4L_tT/g^2$, this tells us

that

$$\frac{\partial}{\partial T}\left(\frac{F_w}{T}\right) = \frac{\partial}{\partial T}\left(\frac{L_y}{L_t}\frac{\sigma(T)}{T^2}\right) \geq 0. \tag{107}$$

Here we have used the definition of the domain wall surface tension:

$$F_w = aL_y\sigma. \tag{108}$$

From (107) we immediately deduce that $\sigma(T) \propto T^\delta$, where $\delta \geq 2$, ignoring possible logs. At the same time we expect that it cannot increase faster than T^3. The perturbative value for the exponent is, as we have seen, $\delta = 2.5$. So we see that our qualitative observations already constrain the temperature variation of the surface tension to lie in the interval $\delta = 2.5 \pm 0.5$. In the quantitative comparisons below we shall attempt to make the comparison with perturbation theory much more precise.

Before doing so it is interesting to ask what the above T^2 bound means physically. The following is a simple heuristic interpretation. Let m_D be the screening mass; then the wall will have a thickness $O(1/m_D)$. A very crude expectation is that $\sigma \propto T^3/m_D$. Now if m_D grows faster than T then it cannot be thermally excited and the whole high-T picture of a screened plasma breaks down. The statement that m_D grow no faster than T is equivalent to our bound that σ grows at least as fast as T^2.

We now turn to a quantitative analysis of the results displayed in Table 4. We recall that the leading order perturbative result is

$$\sigma = \frac{\alpha}{g}T^{2.5} \tag{109}$$

The important energy scale is T and the dimensionless expansion parameter on this scale is g^2/T. Thus the above leading order perturbative result should become exact in the $T \to \infty$ limit. Naively one might expect finite temperature corrections to (109) to be $O(g^2/T)$ - as in 4 dimensions - but here in d=2+1 there might well be logarithms and the power itself might be different. We shall see below that this uncertainty about the functional form of the leading corrections will limit the precision with which we can test perturbation theory. As we have seen, (109) is valid both in the continuum and on the lattice, except that in the latter case the value of the constant α will receive calculable lattice spacing corrections. Since T is the (largest) important physical energy scale, we expect that the lattice spacing corrections should depend only on $aT \equiv 1/L_t$. Moreover, since α is a dimensionless

physical quantity we expect, on quite general grounds for a pure gauge theory, that the corrections should be $O(a^2T^2) \sim O(1/{L_t}^2)$ for small enough a. The detailed perturbative calculations do in fact bear out this expectation.

From (101,108,109) we obtain

$$S_w = \frac{\partial}{\partial\beta}\left(\frac{F_w}{T}\right) = \frac{\alpha L_y}{8{L_t}^2}\left(\frac{g^2}{T}\right)^{1/2} \tag{110}$$

to leading order in perturbation theory. We have calculated the value of α as a function of $aT \equiv 1/L_t$, using lattice perturbation theory (60) and show a selection of these values in Table 8. Since the lattice spacing corrections depend on L_t, we shall mostly examine the T dependence at fixed L_t. Indeed, we have chosen our parameters with this in mind. However before doing so we briefly take the alternative approach of varying L_t at fixed β. For this purpose it is useful to rewrite (110) in the form

$$\frac{S_w}{L_y} = 2\frac{\alpha(L_t)}{\beta^2}\left(\frac{T}{g^2}\right)^{3/2} \tag{111}$$

Now, as we see in Table 4, it is only for $\beta = 75.0$ that we have a usefully large range of L_t values. So we plot these values of S_w/L_y against $T/g^2 \equiv \beta/4L_t$, in Fig. 7. We use logarithmic scales so that a power dependence in T will appear as a straight line. And, indeed, the calculated values do fall on a straight line to a good approximation. The slope suggests a variation $\propto T^{1.6}$ which is close to the perturbative variation of $\propto T^{1.5}$. To carry the comparison further we need to take into account the fact that in addition to the predicted $T^{1.5}$ behaviour, there are different aT lattice corrections at the different values of L_t. That is to say, the behaviour predicted by perturbation theory is $\propto \alpha(L_t)T^{1.5}$ and not just the power of T. In Fig. 7 we show the complete leading order perturbative prediction and we see that its variation fits that of our data very well. The normalisation is not exactly right — but the difference is small and is decreasing with increasing T just as one would expect from a higher order correction in g^2/T. If we do indeed try to fit the data with a higher order correction we find that an $O(g^2/T)$ correction will not work; but

$$\sigma = \frac{\alpha}{g}T^{2.5}\left(1 + 0.13\left(\frac{g^2}{T}\right)^{0.5}\right) \tag{112}$$

fits perfectly well. The precise power of the correction is not to be taken too seriously of course; it may be an effective power that partially simulates the effects of logarithms in our limited range of T/g^2 (this range being roughly 3 to 10).

We conclude from the above comparison that at temperatures $T/g^2 \geq 3$ the T dependence of σ is very close to the perturbative expectation of $T^{2.5}$; indeed what we find is $\sim T^{2.6}$. Moreover this slight difference almost entirely disappears when we include the perturbatively calculated aT corrections to α. The remnant discrepancy, a few percent, decreases as T increases and so is consistent with being a higher order perturbative correction, as, for example, in (112). Unfortunately the fact that we do not know the precise functional form of this correction, prevents us from carrying out the quantitative comparison any further than this.

We turn now to consider the bulk of our calculations. We shall consider the T dependence at fixed values of $L_t \equiv 1/aT$, so that the lattice spacing corrections do not vary with T. At the same time, by performing calculations for several values of aT we can see whether the perturbative predictions show any sign of failing as one approaches the continuum limit. To compare our results to the perturbative prediction we define a quantity $\alpha_{\rm eff}$ by

$$\alpha_{\rm eff} = \frac{\beta^2}{2}\left(\frac{g^2}{T}\right)^{3/2}\frac{S_w}{L_y} \tag{113}$$

As we see from (111), to leading order in perturbation theory $\alpha_{\rm eff}(L_t) = \alpha(L_t)$. In Fig. 8 we display our Monte Carlo results for $\alpha_{\rm eff}$ as a function of g^2/T. The perturbative value of α is also shown, as a horizontal broken line, in each case. We observe that the calculated surface tension indeed approaches the perturbative value as T increases. At the highest values of T the discrepancy is no more than a few percent. Our data is clearly compatible with the leading perturbative result being exact in the $T \to \infty$ limit.

In Fig. 9 we plot the ratio $\alpha_{\rm eff}/\alpha$ for all our data. We see that to a good approximation it is a function only of g^2/T. This supports the idea that the small differences we see between the full and perturbative surface tensions are in fact due to higher order corrections in g^2/T. We note that these higher order corrections are small over our whole range of T. Indeed, even for $g^2/T \sim 1.1$ the correction is only about 25% of the leading term. Recall that this temperature corresponds to only about twice the deconfining

temperature. It is quite extraordinary that lowest order perturbation theory should still be so accurate at such low temperatures.

If we knew the functional form of the leading correction, we would attempt to extrapolate our 'measured' values to $T = \infty$. Unfortunately we do not. In $d = 3 + 1$ we would expect the correction to be simply $\propto g^2/T$. However in $d = 2 + 1$ there are infrared logarithms which may also resum into a power of g^2/T. So it seems reasonable that the correction should be some effective power of g^2/T that lies between 0.5 and 1 in our range of T. If we fit our data with a form

$$\sigma = \frac{\alpha}{g} T^{2.5} \left(1 + c \left(\frac{g^2}{T} \right)^{\varepsilon} \right) \tag{114}$$

then we find that while $\varepsilon = 1$ is excluded, powers near $\varepsilon = 0.65$ work perfectly well, as we see in Fig. 10. The intercepts of these fits are compatible with the leading order perturbative predictions.

The final question in this context is whether there is any sign that this agreement with perturbation theory breaks down as we approach the continuum limit. The above detailed comparisons have involved reducing the lattice spacing by a factor of 2, i.e. from $aT = 1/2$ to $aT = 1/4$. As we see in Figs 8,9 there is no sign of any lattice spacing dependence other than that calculable in perturbation theory. To go further we also calculated the surface tension with $aT = 1/L_t = 1/6$ at $\beta = 75$. In Fig. 11 we show the value of $\alpha_{\rm eff}/\alpha(L_t)$ for this $L_t = 6$ point as well as for other L_t values at approximately the same temperature (using $T/g^2 = \beta/4L_t$). Note that since the T dependence of this quantity is very weak, as we have seen in Fig. 8, it is not important to get T exactly the same at different values of L_t. Note also that this is a reasonably high value of T at which to perform such a test: the deviations from leading order perturbation theory are only at the 7% level or so. We see from Fig. 11 that there is no significant deviation from perturbation theory with decreasing a even down to $aT = 1/6$. It therefore seems extremely unlikely that the *continuum* surface tension will not be equally well described by perturbation theory.

So far we have focused on the surface tension of the domain wall. However perturbation theory also makes predictions for more detailed aspects of the domain wall, such as its profile. In Fig. 12 we show how these predictions compare with our Monte Carlo calculated Polyakov loop profiles for several parameter values. We see very good agreement with the main discrepancy

arising from the fact that the vacuum values of Polyakov loops are ± 1 in leading order perturbation theory. This is primarily an artifact arising from the fact that $\langle\theta\rangle = 0$ does not mean that $\langle\cos\theta\rangle = 1$. A less trivial, but almost invisible difference is that the approach to the vacuum at large distances is Gaussian for perturbation theory, but exponential in the full theory.

In Fig. 13 we show some typical examples of profiles of different components of the action density. Again there is very good agreement with perturbation theory.

We turn now to the Debye screening mass, m_D. When we expand the trace of the Polyakov loop the first non-trivial term is $\sim {A_0}^2$ so that we expect correlations of Polyakov loops to receive contributions from the exchange of pairs of screened electric gluons. However, as emphasised by [26], at higher order in the coupling, g^2/T, they also receive contributions from the magnetic gluon and larger numbers of gluons of both kinds. The question naturally arises: which kind of contribution are we seeing when we extract the masses displayed in Table 3? If we expand the normalised correlation function, $C(z)$, of Polyakov loop operators, P, in energy eigenstates

$$\frac{C(z)}{C(0)} = \sum_n c_n \exp\left(-E_n z\right) \tag{115}$$

then the coefficients, c_n, are just the amplitudes squared

$$c_n = |\langle \mathrm{vac}|P|n\rangle|^2 \tag{116}$$

with normalisation $\sum c_n = 1$. From our above discussion we expect c_n to be largest for the state with two screened electric gluons. Of course, for large enough z, the correlation function will be dominated by the lightest energy, E_{min}, irrespective of the value of c_n (as long as it is non-zero), and so we need to check whether the masses we have listed in Table 3 do indeed correspond to states for which c_n is large. In Table 9 we list the overlaps, c_n, for the states whose masses are listed in Table 3. We provide both the overlap onto the best smeared Polyakov loop operator and the overlap onto the simple, unsmeared Polyakov loop operator. We do so for the extreme values of T at each value of L_t. We see that in all cases the normalised matrix element squared is $\geq 79\%$. Given that we expect the magnetic gluon etc contributions to receive relative suppressions that are powers of g^2/T, which is ~ 0.1 at our highest β values, it is clear that the masses we have obtained belong to

states that have no such suppression. We therefore claim that we can read off m_D from Table 3 using $am_D = 0.5am_P$.

As we have already seen, the Debye screening mass is infinite at 1-loop, due to an infrared divergence. These divergences go away if we use non-zero gluon masses in the diagrams and so one can try to do a self-consistent calculation for the mass, m_D. This has been done by D'Hoker [18] who obtains

$$ {m_D}^2 = \frac{g^2 T}{\pi} \left[\ln\left(\frac{T}{m_D}\right) - 1 + O\left(\frac{1}{(\ln(T/m_D))^{\zeta}}\right)\right] \tag{117} $$

where $\zeta > 0$. We see from (117) that m_D/g^2 is a function only of T/g^2. Naively we would, of course, have expected $m_D \sim g\sqrt{T}$ since, as we have seen, that is the scale for the domain wall. And indeed this is the leading T dependence in (117), up to a weakly varying logarithm. However the correction term is down only by logarithms and so we might not be surprised to find the comparison with perturbation theory not as good as for the properties of the domain wall, where the corrections are powers of g^2/T.

In Fig. 14 we plot our masses against T/g^2. What we actually choose to plot is ${m_D}^2/g^2T$ since that way we factor out the supposedly dominant g^2T factor, and so expose the remaining variation more clearly. We also show the leading perturbative prediction as obtained from the first term of (117). The first observation is that the dominant variation of m_D is indeed $\sim gT^{1/2}$. However there is a substantial additional variation which is too strong to be due to corrections that are higher order in g^2/T. Indeed if we try a fit of the form

$$ {m_D}^2 = g^2 T \left(c_0 + c_1 \left(\frac{g^2}{T}\right)^{\varepsilon}\right) \tag{118} $$

we find that it simply does not work, even if we remove the lowest T point from the fit. Indeed, as we see, this additional T variation is quite similar to that obtained from (117). However the normalisation is completely off. Even allowing for the L_t dependence in our values of m_D, there is a discrepancy of about a factor of 3 with perturbation theory. Since the corrections in (117) are only logarithmic we cannot, of course, claim a contradiction with perturbation theory. However it is worrying that there is no trend towards a reduction of the discrepancy even at our highest values of T where $1/\ln(T/g^2) \sim 0.4$. This is in stark contrast to other properties of the domain wall where we found the corrections to leading order perturbation theory to

be small even for $g^2/T \sim 1$.

8 Conclusions

In this paper we have carried out extensive perturbative and Monte Carlo calculations of the high-T domain walls which are associated with the spontaneous breaking of a $Z(N)$ symmetry in $SU(N)$ gauge theories. As we argued, these walls can be viewed as 't Hooft disorder loops which become squeezed once the extent in Euclidean time becomes small enough, as it does at high enough T. Our purpose has been to test high-T perturbation theory and to establish whether these unusual objects do really exist in the Euclidean continuum theory. In order to be able to obtain numerical results of sufficient accuracy to be convincing, we have worked with the simplest theory that one may consider as realistic in this context: the $SU(2)$ gauge theory in 2+1 dimensions.

This kind of calculation is difficult for several reasons. Firstly the potential problems are infrared and it is therefore crucial to make sure that the volumes used are large enough. This means not only doing detailed numerical finite-size studies, but also calculating the appropriate finite-volume corrections in perturbation theory. For example, in this paper we have shown how one can calculate the effects of roughening on these domain walls. Secondly one-loop perturbation theory becomes exact, at best, only in the limit $T \to \infty$. Now at fixed aT the size of the lattice will grow as $T^{1/2}$, in lattice units, simply because the width of the wall is $O(1/T^{1/2})$ in $d = 2 + 1$. This makes it difficult to simultaneously get close to the continuum limit, where aT is small, and to reach very high values of T. For this reason we have performed the perturbative calculations not only for the continuum theory but also for the lattice theory. In this way we can directly compare perturbation theory to the full non-perturbative results one gets from Monte Carlo simulations.

In practice we have carried out simulations for temperatures as high as $\sim 30T_c$, where T_c is the deconfining temperature, and for lattice spacings as small as $1/6T$. (This comparison with $1/T$ is appropriate, since T is the largest important physical energy scale in the problem). At the highest values of T our numerically obtained values of the surface tension agree with the perturbative predictions at the percent level and this is so at all our

values of a. Moreover there is agreement at the 25% level or so, even at temperatures as low as $g^2/T \sim 1$. When we look at the variation with a, over the range $a = 1/2T$ to $1/6T$, we again find excellent agreement with perturbation theory, with not the slightest hint of any anomaly developing as $a \to 0$.

At the same time we have obtained perturbative predictions for the more detailed properties of the wall, such as the action density profile. These calculations agree very well with our simulations. These profiles are interesting in themselves and show, for example, that $\langle B^2 - E^2 \rangle$ — the thermal energy (in Euclidean space) — becomes negative inside the wall (see Section 5).

The only quantity where we fail to find agreement with perturbation theory is for the Debye screening mass. However here the perturbative calculations are not straightforward and the corrections are expected to be a power of $1/\log(T/g^2)$ and not of g^2/T. So there is no good reason to read too much significance into this particular discrepancy.

Our conclusion is that these high-T domain walls are present in the Euclidean theory, exactly as predicted by perturbation theory, both on the lattice and in the continuum. Since these walls are quantum rather than semiclassical objects, they provide a severe testing ground for high-T perturbation theory. Its success here lends strong support to the usual pragmatic assumption that perturbation theory reliably describes gauge theories at high temperatures.

Acknowledgement We are grateful for support under the Oxford Particle Theory Grant GR/K/55752. In addition A.M. is grateful for support from Kobe Steel, the Queen's Trust, AFUW and IFUW; M.S. for a scholarship from Jesus College and support under the grant NSF-PHY92-00148; C.K.A. for the support of the Royal Society Exchange Program. The numerical calculations were performed partly on the RAL Cray YMP under PPARC grant GR/J21408, and partly on alpha workstations in Oxford Theoretical Physics.

References

[1] L.Susskind, Phys. Rev. **D20** (1979) 2610.

[2] A.M.Polyakov, Phys. Lett. **72B** (1978) 477.

[3] T.Bhattacharya, A.Gocksch, C.P.Korthals Altes and R.D. Pisarski, Phys. Rev. Lett. **66** (1991) 998.

[4] V.M.Belyaev, I.I.Kogan, G.W.Semenoff and N.Weiss, Phys. Lett. **B277** (1992) 331.

[5] K.Lee, C.P.Korthals Altes and R.D.Pisarski, Phys. Rev. Lett. **73** (1994) 1754; C.P.Korthals Altes and N.Watson, Phys. Rev. Lett. **75** (1995) 2799.

[6] C.P.Korthals Altes, A.Michels, M.Stephanov and M.Teper, Nucl. Phys. (Proc. Suppl.) **B42** (1995) 517, and A.Michels, D.Phil. Thesis, Oxford, 1995.

[7] S.T. West and J.F. Wheater, Oxford preprint OUTP-96-21P.

[8] K.Kajantie, L.Karkainen and K.Rummukainen, Nucl. Phys. **B357** (1991) 693.

[9] A. Smilga, Ann. of Phys. **234** (1994) 1.

[10] G.'t Hooft, Nucl. Phys. **B153** (1979) 141.

[11] Y. Y. Goldschmidt and J. Shigemitsu, Nucl. Phys. **B200**[FS4] (1982) 149.

[12] T.Bhattacharya, A.Gocksch, C.P.Korthals Altes and R.D. Pisarski, Nucl. Phys. **B383** (1992) 497.

[13] T. Bhattacharya, A.Gocksch, C.P.Korthals Altes and R.D. Pisarski, Nucl. Phys. (Proc. Suppl.) B20 (1991) 305.

[14] J.Kiskis, Phys. Rev. **D51** (1995) 3781, preprint UCD 95-14.

[15] C.P.Korthals Altes, Nucl. Phys. **B420** (1994) 637.

[16] N. Weiss, Phys. Rev. **D24** (1981) 475.

[17] D.J.Gross, R.D.Pisarski and L.G.Yaffe, Rev. Mod. Phys. **53** (1981) 43.

[18] E. D'Hoker, Nucl. Phys. **B201** (1982) 401.

[19] K.G.Wilson, Phys. Rev. **D10** (1974) 2445.

[20] L. Kärkkäinen and K. Rummukainen, Nucl. Phys. B (Proc. Suppl.) **20** (1991) 309.

[21] M. Lüscher, Nucl. Phys. **B180** (1981) 317.

[22] J. Stack and M. Stone, Phys. Lett. **100B** (1981)476.

[23] J. Groeneveld, J. Jurkiewicz, and C. Korthals Altes, Physica Scripta **23** (1981) 1022.

[24] G.'t Hooft, Nucl. Phys. **B138** (1978) 1.

[25] M. Teper, Phys. Lett. **B289** (1992) 115, **B311** (1993) 223, **B313** (1993) 417.

[26] P. Arnold, L. Yaffe, Phys. Rev. **D49** (1994) 3003.

Table 1: Average plaquette on lattices without a twist.

L_t	β	lattice	no. sweeps	$1 - s_{\rm nt}$
2	100.0	30×60	820,000	0.98998945(28)
	75.0	26×50	400,000	0.98664608(71)
	50.0	50×60	400,000	0.97995063(66)
		40×60	240,000	0.97994775(87)
		30×60	200,000	0.979994952(117)
		20×40	440,000	0.97995159(130)
		16×60	400,000	0.97994859(101)
	25.0	30×48	400,000	0.9597749(15)
		20×48	400,000	0.9597747(21)
		12×60	400,000	0.9597749(23)
		12×40	400,000	0.9597752(23)
		12×30	400,000	0.9597734(34)
		12×26	400,000	0.9597801(38)
		12×20	400,000	0.9597755(47)
	15.0	12×24	400,000	0.9326535(71)
	7.0	12×20	400,000	0.8533597(159)
3	112.5	40×80	800,000	0.99109673(14)
	75.00	30×80	360,000	0.98663259(35)
		30×60	800,000	0.98663236(33)
		30×50	196,000	0.98663197(77)
		24×80	200,000	0.98663262(48)
		18×80	200,000	0.98663250(37)
	37.47	18×60	400,000	0.97317001(126)
		18×46	400,000	0.97316810(130)
	22.45	18×46	400,000	0.95504162(204)
	10.27	18×32	400,000	0.9004471(62)
4	99.97	40×80	800,000	0.98997622(15)
	49.95	24×60	800,000	0.97989112(39)
	29.91	24×48	800,000	0.96631709(87)
	13.81	24×40	800,000	0.92634313(179)
5	62.40	30×100	400,000	0.98391671(38)
	37.33	30×80	400,000	0.97304743(54)
6	75.00	36×90	840,000	0.98662597(12)

Table 2: Average plaquette on lattices with a twist.

L_t	β	lattice	no. sweeps	$1 - s_{\rm tw}$
2	100.0	30×80	800,000	0.98987388(26)
	75.0	26×70	400,000	0.98649347(50)
	50.0	50×60	400,000	0.97972630(65)
		30×60	200,000	0.97972542(91)
		20×60	400,000	0.97972801(91)
		16×60	400,000	0.97972622(124)
	25.0	30×48	400,000	0.9593664(15)
		20×48	400,000	0.9593643(21)
		12×60	400,000	0.9594461(23)
		12×48	400,000	0.9593680(29)
		12×40	400,000	0.9592867(25)
	15.0	12×36	400,000	0.9319060(58)
	7.0	12×30	400,000	0.8519115(137)
		12×20	400,000	0.8512002(174)
3	112.5	40×100	650,000	0.99106642(14)
	75.00	30×100	350,000	0.98659536(35)
		30×80	350,000	0.98658592(37)
	37.47	18×60	400,000	0.97307998(106)
	22.45	18×46	400,000	0.95488588(203)
	10.27	18×32	400,000	0.9000855(59)
4	99.97	40×120	800,000	0.98996380(18)
	49.95	24×84	800,000	0.97986529(39)
	29.91	24×64	800,000	0.96627028(56)
	13.81	24×48	800,000	0.92624494(158)
		24×40	400,000	0.92622498(271)
6	75.00	36×130	600,000	0.98662125(13)

Table 3: Masses obtained from correlations of Polyakov loops.

L_t	β	lattice	$a\,m_p$
2	100.0	30×60	0.315(7)
	75.0	26×50	0.352(4)
	50.0	50×60	0.414(5)
		40×60	0.418(6)
		30×60	0.413(6)
		20×40	0.409(6)
		16×60	0.410(5)
	25.0	30×60	0.526(6)
		20×48	0.529(6)
		12×60	0.529(6)
		12×40	0.525(7)
		12×30	0.520(9)
		12×26	0.533(9)
		12×20	0.522(10)
	15.0	12×24	0.632(8)
	7.0	12×20	0.771(7)
3	112.5	40×80	0.2188(44)
	75.00	30×80	0.2586(53)
		30×60	0.2588(50)
		30×50	0.2561(109)
		24×80	0.2508(126)
		18×80	0.2511(97)
	37.47	18×60	0.3351(59)
		18×46	0.3399(66)
	22.45	18×46	0.395(6)
	10.27	18×32	0.489(4)
4	99.97	40×80	0.1897(18)
	49.95	24×60	0.2420(19)
	29.91	24×48	0.2802(23)
	13.81	24×40	0.3411(40)
5	62.40	30×100	0.177(7)
	37.33	30×80	0.2226(42)
6	75.00	36×90	0.1541(23)

Table 4: The action density of the domain wall per unit length and averaged Polyakov loop masses.

L_t	β	S_w/L_y	$a\,m_p$
2	100.0	0.055474(183)	0.315(7)
	75.0	0.064096(365)	0.352(4)
	50.0	0.08048(22)	0.4123(25)
	25.0	0.11773(38)	0.5269(27)
	15.0	0.1615(20)	0.632(8)
	7.0	0.2598(29)	0.771(7)
3	112.5	0.02728(18)	0.2188(44)
	75.00	0.03342(30)	0.2572(32)
	37.47	0.04811(76)	0.3372(44)
	22.45	0.06448(119)	0.395(6)
	10.27	0.1041(25)	0.489(4)
4	99.97	0.01788(34)	0.1897(18)
	49.95	0.02604(56)	0.2420(19)
	29.91	0.03595(80)	0.2802(23)
	13.81	0.05661(119)	0.3411(40)
5	62.40	-	0.177(7)
	37.33	-	0.223(4)
6	75.00	0.01104(41)	0.1541(23)

Table 5: The action density of the domain wall as a function of the lattice length, L_z, for selected values of β and L_t.

β	L_t	L_z	S_w/L_y
25	2	60	0.11840(101)
		48	0.11722(96)
		40	0.11719(71)
		30	0.11792(84)
		26	0.11497(77)
		20	0.06947(84)
50	2	60	0.07979(36)
		40	0.07877(36)
		34	0.07169(35)
		30	0.04981(52)
		26	0.01735(44)
75	3	100	0.03340(39)
		80	0.03352(32)
		60	0.03239(22)
		54	0.02940(35)
		50	0.02354(44)
		46	0.01577(44)
		40	0.00640(60)

Table 6: Some additional values of the action density of the domain wall, for values of L_z smaller than in Table 2.

L_t	β	L_z	S_w/L_y
2	100.0	60	0.05498(18)
	75.0	50	0.06391(28)
	15.0	24	0.1603(14)
3	112.5	60	0.02701(16)
	37.47	40	0.04863(66)
4	99.97	80	0.01688(26)
	49.95	60	0.02054(58)
	29.91	48	0.03557(82)

Table 7: Variation of the action density of the domain wall and Polyakov loop masses with the length, L_y, of the wall.

β	L_t	L_y	S_w/L_y	$a\,m_p$
25	2	30	0.11765(59)	0.529(3)
		20	0.11820(86)	0.529(5)
		12	0.1184(10)	0.529(6)
		8	0.1162(15)	0.492(11)
		4	0.1091(21)	$\leq$ 0.384(9)
50	2	50	0.08076(34)	0.396(12)
		40	-	0.416(4)
		30	0.08068(53)	0.410(10)
		20	0.07991(61)	0.409(6)
		16	0.08005(58)	0.386(15)
		12	0.07937(64)	0.375(9)
		8	0.07860(65)	0.335(8)
		4	0.07870(179)	0.272(12)
75	3	120	0.03271(54)	-
		60	0.03409(47)	-
		30	0.03347(28)	-
		24	-	0.251(13)
		18	-	0.251(7)
		12	0.03303(65)	0.218(7)
		6	-	$\leq$ 0.183(6)

Table 8: Perturbative values of the constant, α, in the interface tension.

L_t	α
2	6.024
3	5.655
4	5.409
5	5.284
6	5.221
8	5.165
10	5.142
20	5.113
∞	5.104

Table 9: Overlaps of Polyakov loop operators onto the states coresponding to our values of m_p.

L_t	β	$O_{\rm best}$	$O_{\rm Bl=1}$
2	100.0	0.88	0.81
	25.0	0.93	0.82
	7.0	0.98	0.90
3	112.5	0.84	0.79
	10.27	0.98	0.89
4	99.97	0.92	0.81
	13.81	0.97	0.86
6	75.00	0.89	0.80

Figure 1: Location of the twist. The plaquettes that are indicated will appear with a factor of -1 in the twisted action.

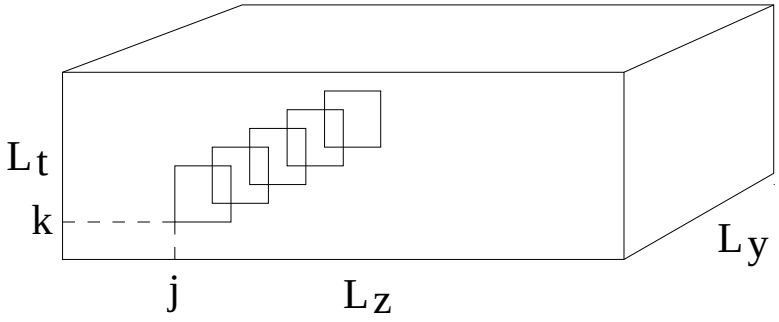

Figure 2: Values of Polyakov loops on typical field configurations with a domain wall: for $L_t = 2$ at: (a) $\beta = 100$, (b) $\beta = 7$.

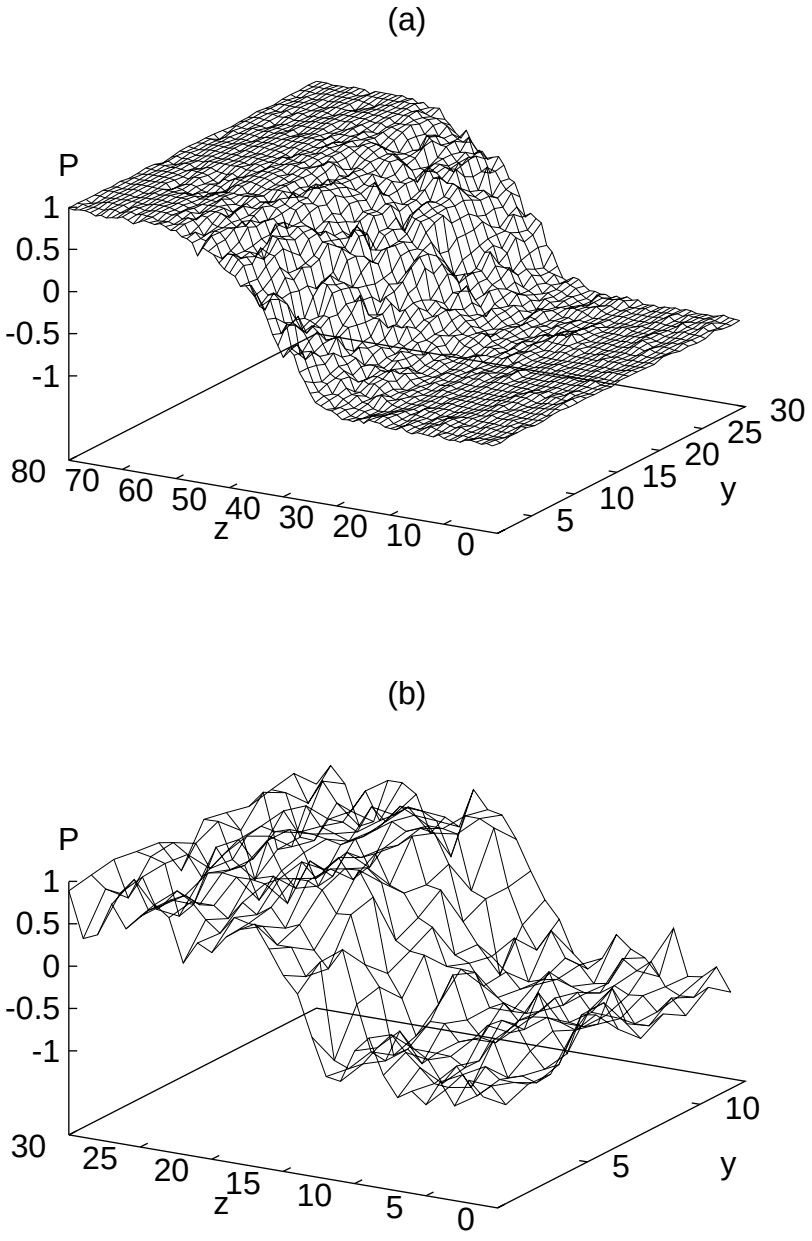

Figure 3: Effective masses from Polyakov loop correlations (+) and from the tails of domain walls ($\diamond$) for (a) $\beta = 112.5$ with $L_t = 3$, (b) $\beta = 25$ with $L_t = 2$.

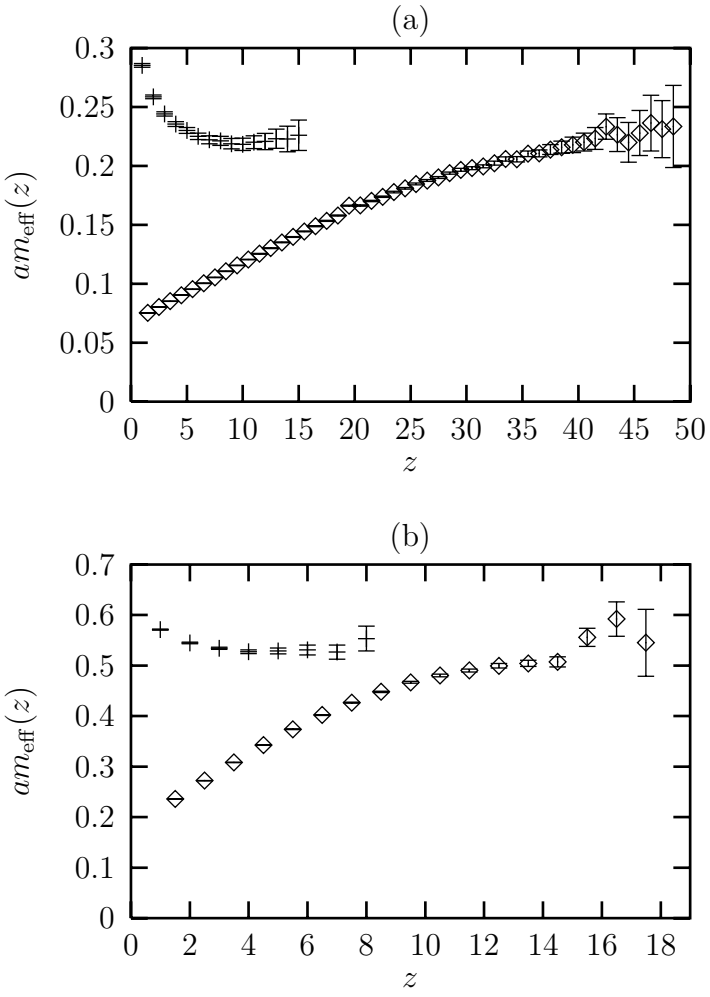

Figure 4: Dependence of the domain wall action density on the (scaled) length of the lattice. Plotted are the values in Table 5 and the lines are the leading order perturbation theory expectation (see text).

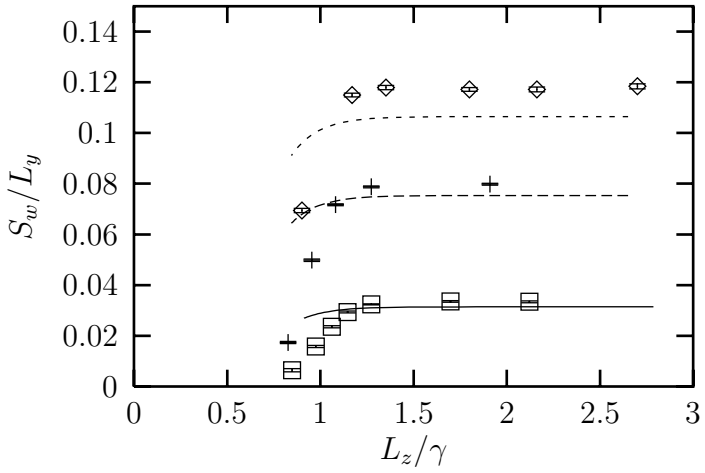

Figure 5: The width of the domain wall as a function of the length of the lattice for (a) $\beta = 75$ and $L_t = 3$, (b) $\beta = 25$ and $L_t = 2$. Widths are calculated when the Polyakov loop attains 2/3 ($\diamond$) and 9/10 (+) of its vacuum value.

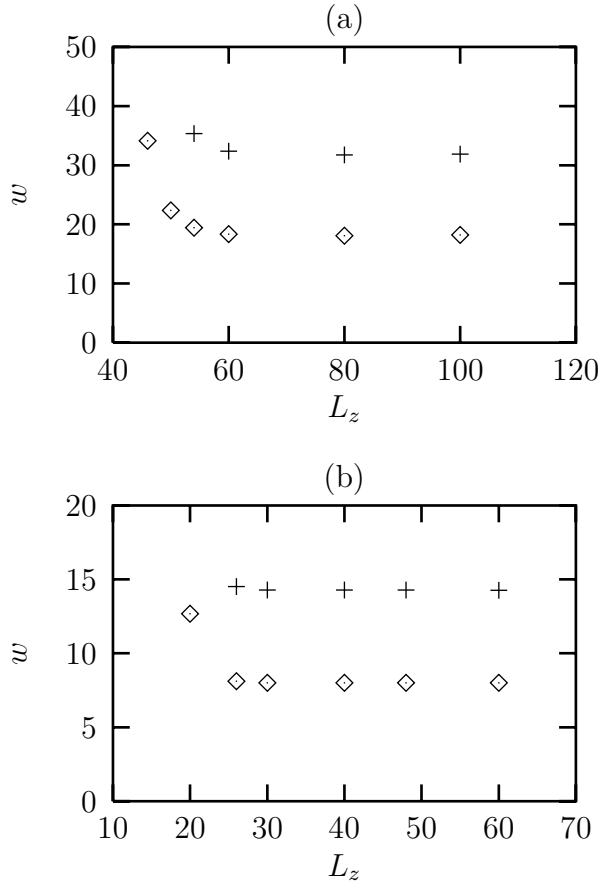

Figure 6: Widths of the domain wall (defined as in Fig. 5) plotted against $\gamma = \pi(\beta L_t)^{1/2}$ for (a) $L_t = 2$, (b) $L_t = 3$, (c) $L_t = 4$. Lines are corresponding perturbative predictions; the dotted lines in (c) are for the continuum, $L_t = \infty$.

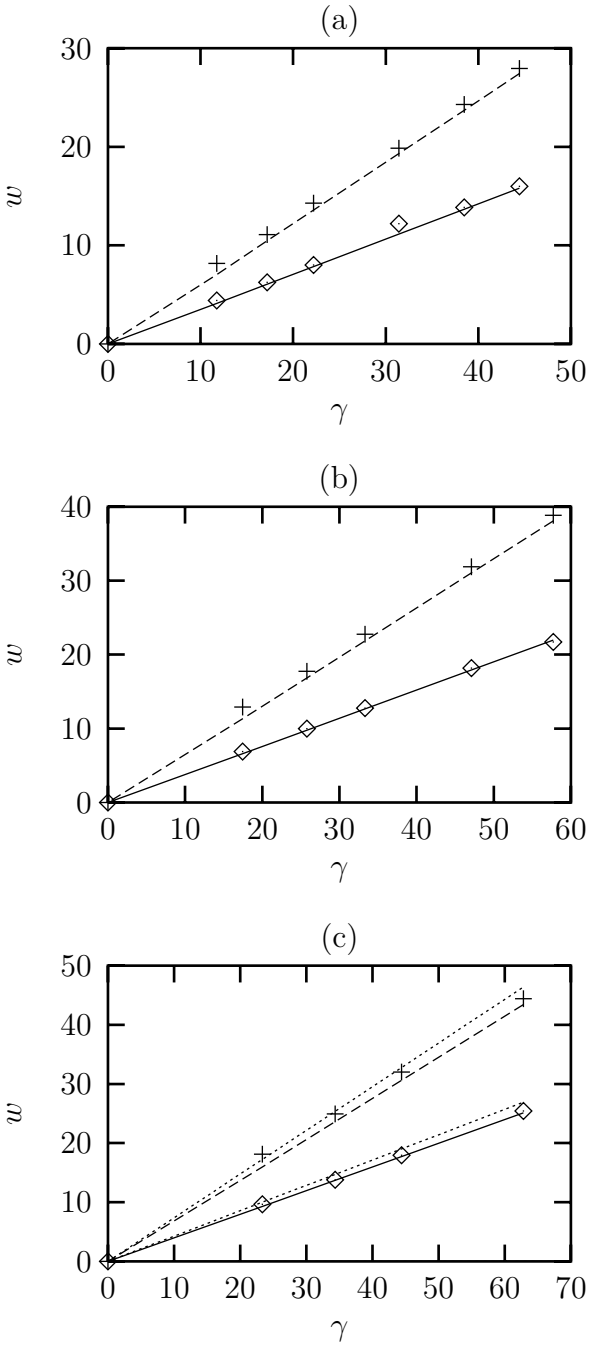

Figure 7: Action density of the domain wall ($\diamond$) for $L_t = 2, 3, 6$ at $\beta = 75$. The line is a fit (see text). Also shown are the perturbative values ($+$) for $L_t = 2, 3, 4, 5, 6$.

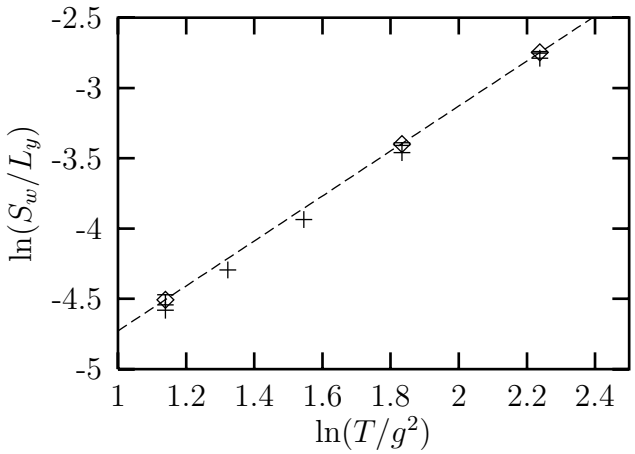

Figure 8: The interface tension (with the factor $T^{2.5}/g$ removed): numerical values ($\diamond$) compared to leading order perturbation theory (dashed lines).

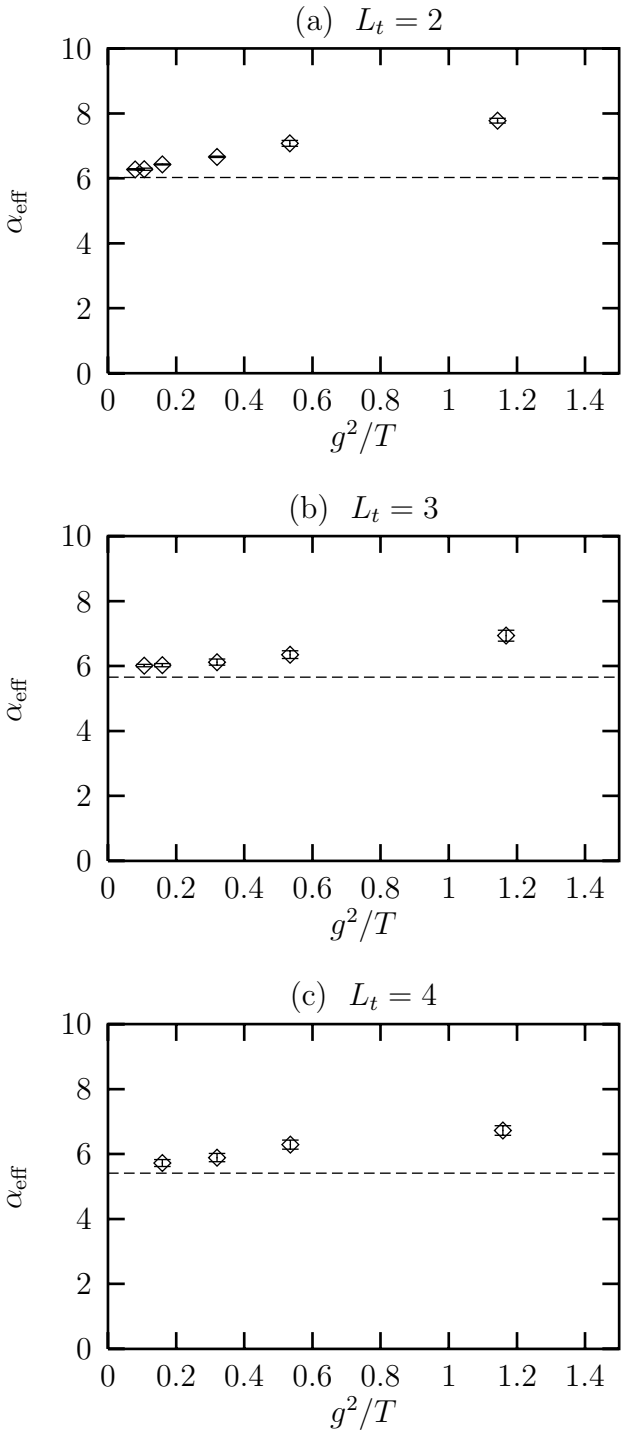

Figure 9: Ratio of numerical and perturbative interface tensions versus the high-T expansion parameter, g^2/T.

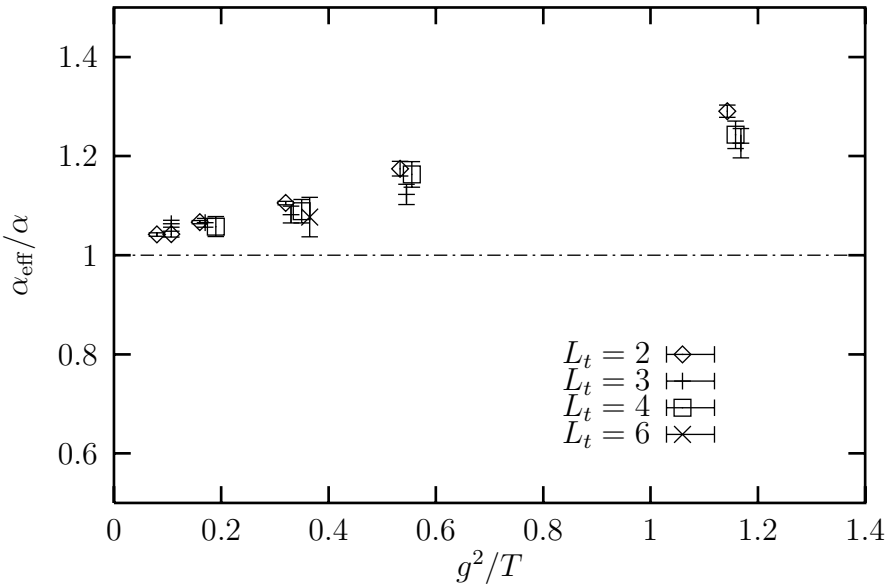

Figure 10: Trial extrapolations to the $T = \infty$ limit of the calculated interface tensions.

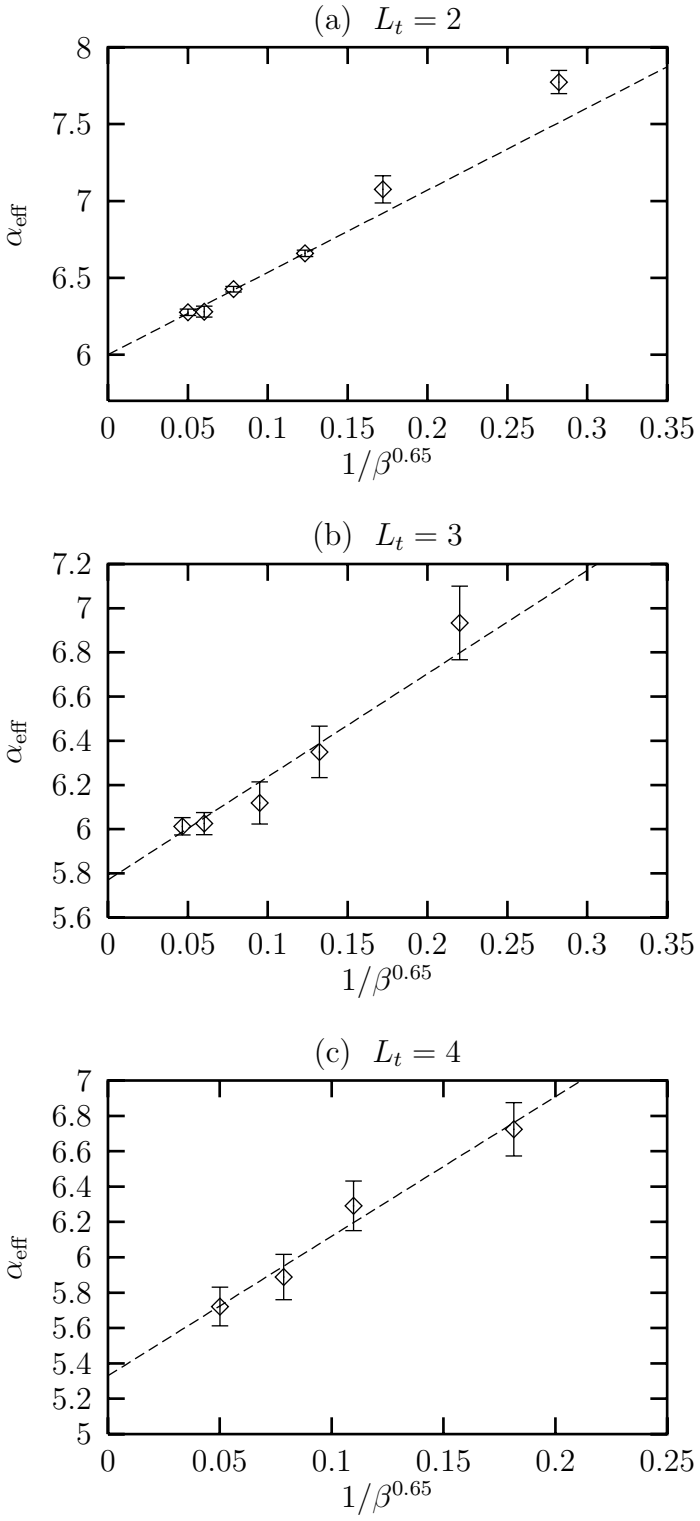

Figure 11: Ratio, at fixed T, of numerical and (leading-order) perturbative interface tensions for decreasing lattice spacing ($a \equiv 1/L_t T$).

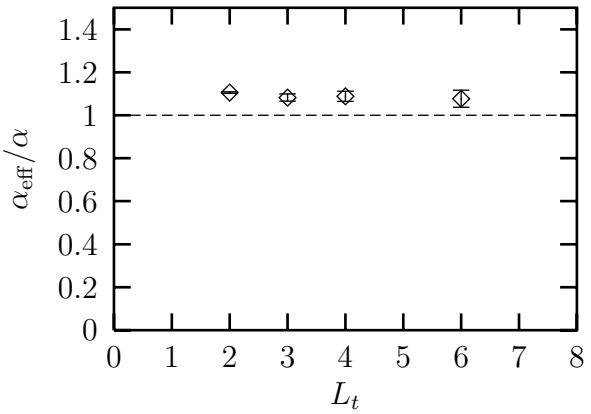

Figure 12: Profile of the Polyakov loop within the domain wall (centred at $z = 0$): numerical values (solid lines) and perturbation theory (dashed lines).

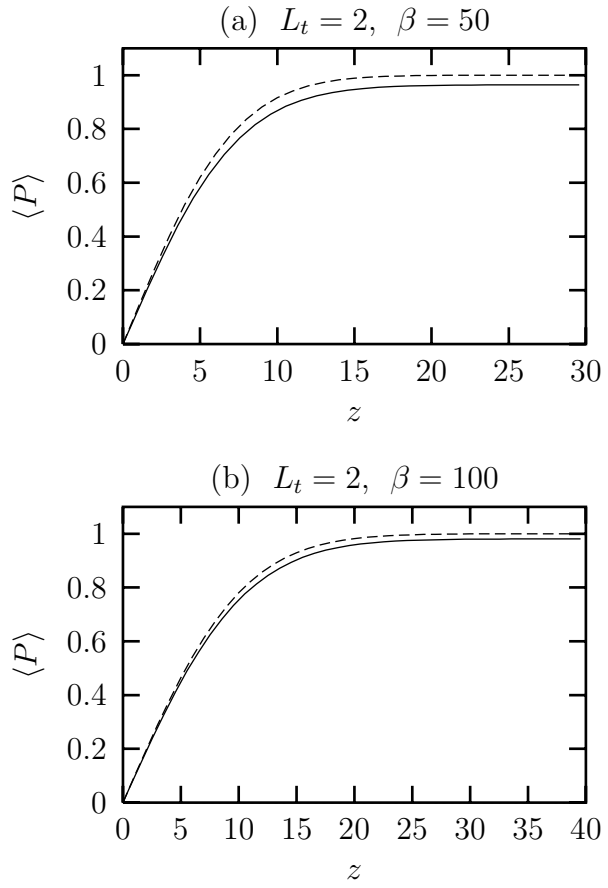

Figure 13: Vacuum-subtracted local action densities within the domain wall: numerical calculations at $\beta = 99.97$ and $L_t = 4$, compared with perturbation theory (lines).

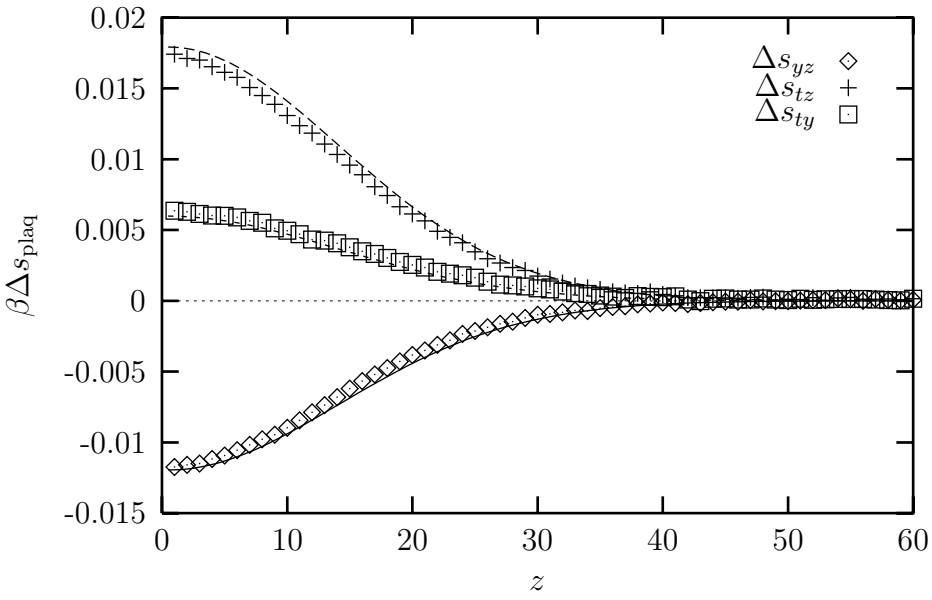

Figure 14: Numerically calculated values of the Debye mass, compared to D'Hoker's self-consistent perturbative prediction.